

Wright State University

CORE Scholar

[Browse all Theses and Dissertations](#)

[Theses and Dissertations](#)

2021

Effect of Cloud Cover on Optimum Orientations of Fixed Solar Panels for Maximum Yearly Energy Collection

Prethew Prasad
Wright State University

Follow this and additional works at: https://corescholar.libraries.wright.edu/etd_all



Part of the [Oil, Gas, and Energy Commons](#), and the [Power and Energy Commons](#)

Repository Citation

Prasad, Prethew, "Effect of Cloud Cover on Optimum Orientations of Fixed Solar Panels for Maximum Yearly Energy Collection" (2021). *Browse all Theses and Dissertations*. 2487.
https://corescholar.libraries.wright.edu/etd_all/2487

This Thesis is brought to you for free and open access by the Theses and Dissertations at CORE Scholar. It has been accepted for inclusion in Browse all Theses and Dissertations by an authorized administrator of CORE Scholar. For more information, please contact library-corescholar@wright.edu.

EFFECT OF CLOUD COVER ON OPTIMUM ORIENTATIONS OF FIXED SOLAR PANELS FOR MAXIMUM YEARLY ENERGY COLLECTION

A thesis submitted in partial fulfilment
of the requirements for the degree of
Master of Science in Renewable and Clean Energy Engineering

By

PRETHEW PRASAD
B.Tech., Vellore Institute of Technology, India, 2016

2021
Wright State University

WRIGHT STATE UNIVERSITY
GRADUATE SCHOOL

April 23, 2021

I HEREBY RECOMMEND THAT THE THESIS PREPARED UNDER MY SUPERVISION BY Prethew Prasad ENTITLED Effect of Cloud Cover on Optimum Orientations of Fixed Solar Panels for Maximum Yearly Energy Collection BE ACCEPTED IN PARTIAL FULFILLMENT OF THE REQUIREMENTS FOR THE DEGREE OF Master of Science in Renewable and Clean Energy Engineering.

James Menart, Ph.D.
Thesis Director

Raghavan Srinivasan, Ph.D., P.E.
Chair, Department of Mechanical and
Materials Engineering

Committee on Final Examination:

James Menart, Ph.D.

Mitch Wolff, Ph.D.

Scott Thomas, Ph.D.

Barry Milligan, Ph.D.
Vice Provost for Academic Affairs
Dean of the Graduate School

Abstract

Prasad, Prethew M.S.R.C.E. Department of Mechanical and Materials Engineering, Wright State University, 2021. Effect of Cloud Cover on Optimum Orientations of Fixed Solar Panels for Maximum Yearly Energy Collection.

The amount of cloud cover present in the sky is a significant factor when determining the solar radiation impinging on a solar panel. The optimum tilt required to achieve maximum energy impingement on a surface is also influenced by the amount of cloud cover. This work presents a method for determining the optimum tilt angle for a fixed solar panel when a set amount of cloud cover is present in the sky. Fixed tilt angles that have the most incident solar energy over the course of a year as a function of cloud cover, latitude, and azimuthal angle orientation are calculated for the entire world, the entire range of cloud covers, and the entire range of azimuthal orientations. Maximum intercepted energy is also presented.

A trigonometric, integral equation is derived to determine the optimum tilt angle. This derivation was done as a continuation of prior work performed at Wright State University on optimum panel tilts for no atmosphere and clear sky conditions. The model developed here is different in that it includes the effects of the change of panel sunrise and sunset with panel tilt. In comparing results calculated with this effect to those without, it was determined that including panel sunrise and sunset change with tilt has no significant impact on the optimum tilt angle or intercepted solar energy. This is beneficial because the complexity added to the model by including this effect is substantial.

In addition to deriving a more complete optimum tilt angle equation, clear sky models for beam and diffuse transmissivities from two different sources are combined with cloud cover models from a third source. It is felt that this combination of models results in more realistic beam and diffuse transmissivity models than using the recommended clear sky models. Using this combination of clear sky and cloudy sky transmittance models required adjustments to the cloud cover model. These adjustments are clearly described in this thesis. The resulting model is capable of calculating optimum tilt angles and maximum intercepted solar energy for sky conditions from clear to completely overcast.

Complete results of optimum tilt angles and maximum intercepted energy are presented. A more complete presentation of the effects of cloud cover on optimum tilts has not been found in

the literature. These studies are done for the entire world from the south pole to the north pole as a function of latitude and azimuthal orientation. As expected the results show that increasing cloud cover always reduces the maximum solar energy intercepted, with a faster decrease as the amount of cloud cover increases. The optimum tilt angles decrease as the cloud cover increases, going to a horizontal orientation for completely overcast skies. The highest intercepted energy is always found when the panel is pointing due south in the Northern Hemisphere and due north in the Southern Hemisphere. The optimum tilt angles are also the highest at this azimuthal orientation. As the panel is shifted away from this azimuthal orientation, the optimum tilt angle and the optimum energy values decrease. Near symmetry in the optimum tilt angles and maximum intercepted energy is found between the Northern and Southern Hemispheres and between easterly and westerly orientated panels.

Along with cloud cover conditions that are uniform throughout the year, studies are done on semi-annual cloud changes and semi-daily cloud changes. Semi-annual cloud changes deal with different amounts of cloud cover over the two halves of the year, the winter half and the summer half. Semi-daily cloud changes deal with different types of cloud cover before solar noon and after solar noon. Interesting results are obtained with these cloud cover profiles.

Table of Contents

Chapter 1 Introduction	1
1.1. Benefits of Solar Energy Collection	1
1.2. Methods of Orienting Solar Panels	4
1.2.1. Two-Axis Tracking	4
1.2.2. Single-Axis Tracking.....	5
1.2.3. Fixed Panels.....	6
1.2.3.1. Roof Mounted Solar Panels	7
1.2.3.2. Ground Mounted Solar Panels.....	8
1.2.3.3. Fixed Panels versus Two and One-Axis Trackers.....	8
1.3. Optimum Solar Panel Orientation Work Done at Wright State.....	9
1.4. Goals and Outline of Thesis	12
1.4.1. Literature Survey.....	12
1.4.2. Derivation of Clear Sky Optimum Tilt Equation	12
1.4.3. Transmissivities that Include Cloud Effects.....	13
1.4.4. Results for Entire World.....	13
1.4.5. Conclusions	14
Chapter 2 Connections to Others Work.....	15
2.1. Sky Models	15
2.2. Transmissivity Models.....	17
2.2.1. Clear Sky Transmissivity Models	18
2.2.2. Cloudy Sky Transmissivity Models	19
2.3. Optimum Tilt Studies around the World	20
2.4. Research Done at Wright State University	23
Chapter 3 Derivation of Optimum Tilt Equation.....	27
3.1. Solar Incidence Energy	28
3.2. Optimum Tilt Angle Equation.....	32
3.3. Rate of Change of Panel Sunrise and Sunset Times with Panel Tilt.....	38
Chapter 4 Atmospheric Transmissivities.....	40
4.1. Definitions of Beam and Diffuse Transmissivities.....	41

4.2. Clear Sky Transmissivities	42
4.3. Cloudy Transmissivities	46
4.4. Adjustments to Kasten and Czeplak Model	48
Chapter 5 Results	51
5.1. Effect of Derivative of the Integral Terms.....	53
5.2. Uniform Cloud Cover throughout the Year.....	55
5.3. Semi-Annual Cloud Changes	64
5.4. Semi-Daily Cloud Changes.....	65
Chapter 6 Conclusions	70
6.1. Model Innovations	70
6.2. Optimum Tilt Angle and Incident Solar Energy Results	72
References	75

List of Figures

Figure 1.1: Cost of producing a MW-h of electricity from conventional and renewable energy sources. [2].....	3
Figure 1.2: Schematic showing panel and sun angles [5].....	7
Figure 4.1: Clear sky beam transmissivities from the model of Hottel [24] and from the model of Kasten and Czeplak [17] for June 21, at a latitude of 40°.	44
Figure 4.2: Clear sky diffuse transmissivities from the model of Liu and Jordan [18] and from the model of Kasten and Czeplak [17] for June 21, at a latitude of 40°.	44
Figure 4.3: Transmissivities determined from the model developed in this work for June 21, at a latitude of 40° where the cloudy results are at 4 oktas.	50
Figure 4.4: Transmissivities determined from the model developed in this work for December 21, at a latitude of 40° where the cloudy results are at 4 oktas.	50
Figure 5.1: Yearly optimum tilt angles for a uniform value of N = 0 throughout the year.	56
Figure 5.2: Yearly maximum intercepted energy for a uniform value of N = 0 throughout the year.	56
Figure 5.3: Yearly optimum tilt angles for a uniform value of N = 2 throughout the year.	57
Figure 5.4: Yearly maximum intercepted energy for a uniform value of N = 2 throughout the year.	57
Figure 5.5: Yearly optimum tilt angles for a uniform value of N = 4 throughout the year.	58
Figure 5.6: Yearly maximum intercepted energy for a uniform value of N = 4 throughout the year.	58
Figure 5.7: Yearly optimum tilt angles for a uniform value of N = 6 throughout the year.	59
Figure 5.8: Yearly maximum intercepted energy for a uniform value of N = 6 throughout the year.	59
Figure 5.9: Yearly optimum tilt angles for a uniform value of N = 8 throughout the year.	60

Figure 5.10: Yearly maximum intercepted energy for a uniform value of $N = 8$ throughout the year. 60

Figure 5.11: Optimum tilt angles for semi-annual varying values of N 66

Figure 5.12: Yearly maximum intercepted energy for semi-annual varying values of N 66

Figure 5.13: Optimum tilt angles for semi-daily varying values of N 68

Figure 5.14: Maximum intercepted energy for semi-daily varying values of N 68

List of Tables

Table 2.1: Some models that have been used to determine the amount of solar insolation on a tilted surface including the effects of the atmosphere..... 17

Table 2.2: Some beam transmissivity models..... 18

Table 2.3: Some diffuse transmissivity models..... 18

Table 2.4: Karkee et al’s. [38] optimum tilt angle results for different periods of the year..... 21

Table 2.5: Yearly optimum tilt angle results for several locations..... 22

Table 2.6: Selected optimum tilt angle results of Nakrani [8] and Medarapu [9] for Dayton, Ohio (39.83°N latitude, 84.06°E longitude). Note that positive azimuthal angles point west..... 24

Table 5.1: Comparisons of optimum tilt and maximum incident energy results without the derivative of the integral terms and with the derivative of the integral terms for -90/90 azimuthal angles and $N = 0$ 54

Table 5.2: Comparisons of optimum tilt and maximum incident energy results without the derivative of the integral terms and with the derivative of the integral terms for -90/90 azimuthal angles and $N = 4$ 55

Table 5.3: Effect of cloud cover on optimum tilt angles for different amounts of uniform cloud cover throughout the year..... 63

Table 5.4: Effect of cloud cover on maximum incident energy for different amounts of uniform cloud cover throughout the year..... 63

Nomenclature

I_T	Total hourly radiant energy impinging on a tilted surface
I_b	Beam radiation impinging on a horizontal surface
I_d	Diffuse radiation impinging on a horizontal surface
I_g	Global radiation impinging on a horizontal surface
G_T	Instantaneous power impinging on tilted surface
G_b	Instantaneous solar beam radiation impinging on horizontal surface
G_d	Instantaneous solar diffuse radiation impinging on horizontal surface
G	Instantaneous total solar radiation impinging on horizontal surface
G_{cs}	Instantaneous total solar radiation impinging on horizontal surface for clear sky condition
$G_{b,cs}$	Instantaneous solar beam radiation impinging on horizontal surface for clear sky condition
$G_{d,cs}$	Instantaneous solar diffuse radiation impinging on horizontal surface for clear sky condition
G_{on}	Variation of the solar constant as a function of day number
G_{sc}	Solar constant
k	Clearness index
Y_{tot}	Integration of instantaneous power over the year
ρ	Reflectivity of the ground
ρ_g	Reflectivity of the ground
R_B	The ratio of total solar radiation impinging on tilted surface to that radiation impinging on horizontal surface
β	Optimum tilt angle of the solar panel
γ	Azimuthal angle of the solar panel
ϕ	Latitude angle
δ	Declination angle
δ_{sr}	Declination angle at sunrise
γ_s	Solar azimuthal angle

θ	Solar incidence angle
A_c	Area of the solar panel collector plate
τ_b	Beam transmissivity
τ_d	Diffuse transmissivity
$\tau_{b,cs}$	Beam transmissivity of clear sky
$\tau_{d,cs}$	Diffuse transmissivity of clear sky
$\tau_{b,cc}$	Beam transmissivity of cloudy sky
$\tau_{d,cc}$	Diffuse transmissivity of cloudy sky
θ_z	Solar zenith angle
ω	Hour angle
ω_{sr}	Hour angle at sunrise
t_{ss}	Actual sunset time
t_{sr}	Actual sunrise time
t_{sse}	Sunset time on earth
t_{sre}	Sunrise time on earth
t_{ssp}	Sunset time on panel
t_{srp}	Sunrise time on panel
n_d	Day number of the year
t_d	Solar time
N	Okta number
$a_0, a_1, \text{ and } k$	Constants for Hottel's beam transmittance model
$A \text{ and } B$	Constants for ASHRAE beam transmittance model

Acknowledgements

I would like to thank my thesis advisor Dr. James Menart, the Director of the Renewable and Clean Energy Master's Degree Program at Wright State University for his guidance throughout the course of my thesis. It took a lot of patience on his part to get this work finished and up to the mark. I would like to thank all the faculty members of the Mechanical and Materials Science department for guiding me on the right path. I would also like to thank Dr. Mitch Wolff and Dr. Scott Thomas for being a part of my thesis defence committee.

I want to thank my parents and relatives who are back home in India. They have been waiting patiently for me to complete my master's degree. I am always kept in their prayers and I have felt the effect of those prayers though I am thousands of miles away from home. I also want to thank my friends back home who continuously provided emotional support to me over the past few years.

I want to thank my friends here at the university and outside the university for all the help provided to me whenever I asked for it. It was a big change for me to travel abroad to pursue my education and they were my family far away from home. They helped me with my home sickness. I never felt like I was so far away from home.

Finally, I would like to thank God Almighty for always looking over me and guiding me on this path filled with knowledge and education. Whenever I strayed from this path, he pulled me back and without his help I would not be at this amazing position I am in right now.

Chapter 1

Introduction

1.1. Benefits of Solar Energy Collection

Conventional sources of energy, like fossil fuels, are limited in supply and thus there will come a time when they are exhausted or the price to extract them from the ground becomes prohibitive. While there are ample supplies of fossil fuels available at the present time, an ever-growing population will put strains on these types of energy sources. The world needs energy sources that do not have limits. This is the case with renewable energies because they continually replenish themselves.

The world also has a need for energy sources that do not alter the environment to a significant degree. This can be satisfied with renewable energies. It is well known that the burning of fossil fuels injects many harmful substances into the environment like sulphur dioxide, nitrogen oxides, carbon monoxide, mercury, soot, polycyclic aromatic hydrocarbons, other volatile chemicals, and carbon dioxide [1]. Sulphur dioxide contributes to acid rain, nitrogen oxides produce smog, carbon monoxide and mercury are poisonous to humans, soot or small airborne particulate matter can cause lung problems, the volatile chemicals form ground level ozone, and carbon dioxide is targeted as being a major cause of global warming. All of these harmful chemicals are reduced or eliminated with a number of renewable energy sources.

In a perfect world, we should switch to renewable energy sources immediately. Since that is not practical, the switch from conventional sources of energy to renewable energy sources should be carried out gradually. It is seen that many countries around the world are adopting this

ideology and moving forward with this strategy. Humanity has declared its readiness to transition into a low carbon economy.

In the author's opinion the sun is one of the best forms of renewable energy to adopt. Since the sun shines on the earth whether we harness its energy or not, using solar energy causes no change to the earth's ecosystem. While some may think using too much solar energy will reduce the temperature of the earth, this is not the case. If the sun's energy is first converted to electricity, once the electricity is used it gets converted back to heat. This same thing happens to all the sun's energy when it is absorbed by the earth. By using solar energy to produce electricity before being converted into heat, we are simply adding an intermediate step to the natural degradation of solar energy from electromagnetic energy to low temperature thermal energy (heat). This means humankind can harvest solar energy for electric power production with no change to the natural environment.

Another reason for switching to solar energy to meet humankind's energy needs, is the sun is essentially a never-ending source of energy. It has been estimated that enough solar energy reaches the earth in one hour to supply all the earth's energy needs for an entire year [1]. Since the sun will deliver this energy for the next 5 billion years [1], there is no worry of running out of solar energy. In the present day, where there is an exponential increase in yearly energy demand, solar energy is one of the easiest renewable energy sources to harvest. Solar energy can be collected by special panels and converted to thermal energy. This thermal energy can be used to heat homes and buildings or converted into electrical energy utilizing turbines and generators. An even more beneficial means of collecting solar energy is with photovoltaic panels. Photovoltaic panels use semiconductors to directly convert solar energy into electricity.

It turns out that using photovoltaic panels to harness solar energy and convert it to electricity is economically attractive at the present time. Under certain conditions, producing a kilowatt-hour (kW-h) of electricity with solar panels is cheaper than doing so with coal, natural gas, or nuclear energy. According to "Lazard's Levelized Cost of Energy Analysis" [2] for 2020, the cheapest unsubsidized cost for a kW-h of electricity from solar energy is 2.9 cents compared to that from natural gas which is 4.4 cents, coal which is 6.5 cents, and nuclear which is 12.9 cents. The expanded results of Lazard's energy analysis are shown in Figure 1.1. This figure shows that using thin film solar photovoltaic panels to produce electricity is the second cheapest way to produce a kW-h of electricity. Producing electricity from wind is slightly cheaper at the present

time, but price trends indicate that this may flip in the near future. While there are wide ranges to these cost values and they depend on a number of factors, they do indicate that solar is an economical means to generate electrical power at this time. On top of this, solar is becoming cheaper as research finds new and better ways to convert solar energy into electrical energy. This is the ultimate purpose of the research presented in this thesis, to further lower the cost that humankind has to pay to convert solar energy into electrical energy or solar energy into some other form of useful energy. This thesis does this by determining the optimum orientations of fixed solar panels in cloudy and clear sky conditions. How ground based, fixed solar panels are orientated during installation generally does not add to the capital costs, but it does increase the amount of solar energy impinging on the panel. This means more electricity is produced for the same capital costs, making the per kW-h price lower. For cases where panel orientations are not limited, it would be foolish not to orientate fixed solar panels to optimize their useful production. In order to place panels in their optimum orientation, designers and installers must know the optimum orientation. This work develops mathematical models and presents results to increase our knowledge of the optimum orientation of fixed solar panels.

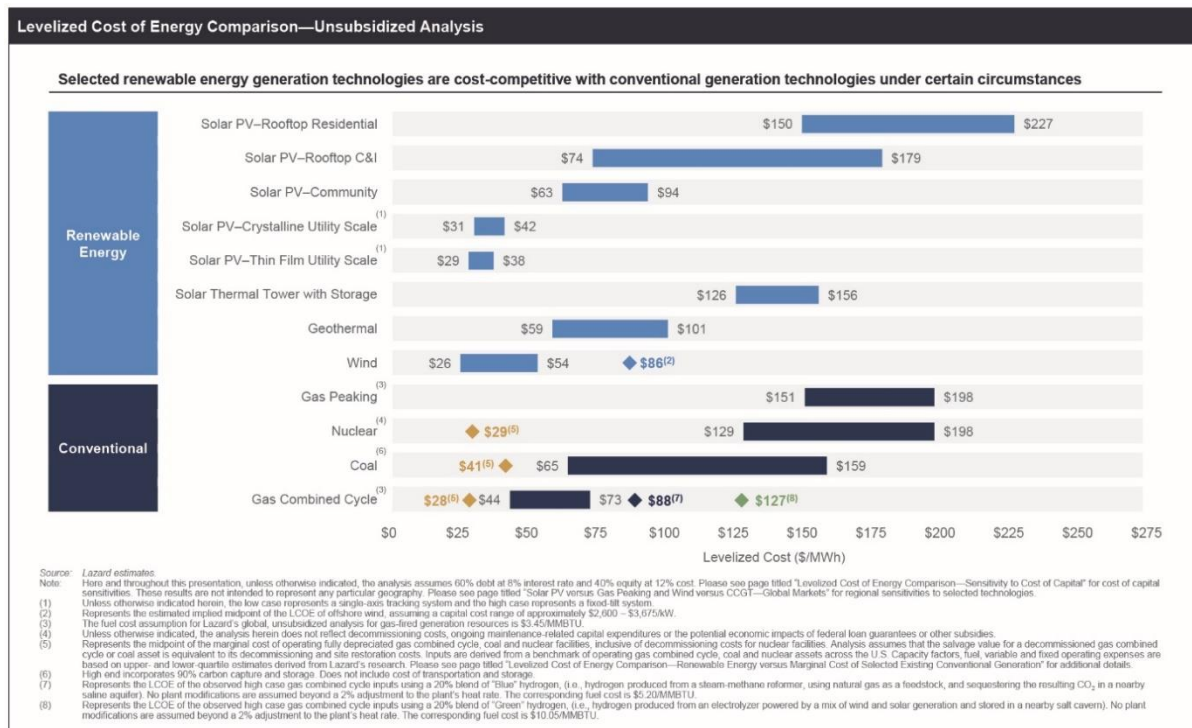


Figure 1.1: Cost of producing a MW-h of electricity from conventional and renewable energy sources. [2]

1.2. Methods of Orienting Solar Panels

Orientation of solar panels is an essential part of the design of a solar installation as it affects the cost of useful energy production and the land area required to meet the energy demand. Because the sun moves relative to a fixed location on the earth, there is no one orientation that provides the maximum solar impingement per unit area of panel for all moments of the day or all days of the year. Maximum solar energy collection will only be obtained if the panel tracks the movement of the sun across the sky as a function of time. There are two basic movements of the sun across the sky when viewed from a fixed location on the surface of the earth. The first basic movement of the sun is from east to west. Of course, this occurs because the earth is rotating, but from a fixed point on the earth it looks like the sun is moving from east to west across the sky. This movement occurs once each day. The second basic movement of the sun is the altitude of the sun in the sky relative to the horizon. This movement occurs over the course of a day and over the course of a year. Of course, the sun is low in the sky at sunrise and sunset and high in the sky at noon, but the sun also changes its altitude in the sky as a function of the time of year. This seasonal altitude change is due to the tilt of the earth relative to its plane of rotation around the sun and the location of the earth in its orbit around the sun. These two motions of the sun have to be addressed when optimizing fixed solar panel orientation.

While this thesis is only concerned with fixed panels, some discussion of moving solar panels is given below. There are three basic categories of tracking for solar panels. These are two-axis tracking, which collects the most solar energy, single-axis tracking, and fixed panels, which collect the least amount of solar energy. The amount of solar energy collected by single axis tracking is somewhere between two-axis tracking and fixed.

1.2.1. Two-Axis Tracking

A two-axis tracking system has two degrees of freedom. Essentially there is an azimuthal axis of rotation and polar axis of rotation. This is the best tracking system as it can track both the east-west movement of the sun, as well as the altitude movement of the sun. This means that the panel can be oriented directly towards the sun at all times during the day and collect the most beam solar radiation. Beam radiation is solar radiation that travels directly from the sun to the surface of the earth without redirection by the surface of the earth or the earth's atmosphere. To capture the maximum beam radiation from the sun, a normal vector from the surface of the panel is made to

be parallel with a line that runs from the center of the panel to the center of the sun. Thus, the panel is orientated so the rays of the sun are normal to the surface of the solar panel. Because of diffuse and ground reflected radiation, this orientation may not provide the maximum collected solar energy, but it will be very close to the maximum. To get the maximum solar energy including beam, diffuse, and ground reflected radiation, the panel can be adjusted slightly to optimize the collection of all three of these components. Two-axis tracking makes these adjustments possible.

1.2.2. Single-Axis Tracking

There are a number of types of single-axis trackers. These types are based on the orientation of the axis around which the panel rotates. Fundamentally this rotational axis can be viewed as a line. The orientation of this line is what gives rise to the different types of single-axis trackers. While there are theoretically and infinite number of orientations of these rotation axes, there are a few key ones that will be mentioned. The first is an east-west single-axis tracker. For this type of tracker, the axis of rotation lies in a horizontal plane and runs in an east-west direction. Solar panels rotating about an east-west axis are capable of tracking the altitude movement of the sun, but not the east-west movement of the sun. Conversely, confining the rotation axis to a north-south direction in a horizontal plane allows panels to track the east-west movement of the sun. While it is generally not done, the rotation axis can be orientated in any direction in a horizontal plane. This would give the panels some ability to capture both motions of the sun, but at the same time it would reduce the panel's ability to completely capture one of the motions of the sun.

Of course, the axis of rotation can be tilted at any angle desired from the horizontal. No tilt and 90 degrees are the two extremes. For all but the vertical case, a tilted axis must be given an orientation as was done in the prior paragraph. The most common axis tilt is tilting the panel upwards from the horizontal the number of degrees of the latitude of the panel's location. Tilting a north-south axis of rotation at an angle equal to the latitude makes the rotation axis parallel to the earth's axis of rotation. This helps minimize the angle of incidence of beam radiation on the panel. There does not appear to be any benefit to tilting an east-west orientated rotation axis. When you tilt an east-west rotation axis up from the horizontal, you limit the panel's ability to track the altitude motion of the sun, with no gain in east-west tracking abilities. For general rotation axis orientations, Marion and Dobos [3] developed equations where the panel is parallel to the axis of

rotation. Marion and Dobos also implemented a rotation angle limit in these equations to stop the panel at rotation angles where it would be shaded by adjacent panels.

Another general orientation of the rotation axis is vertical. The vertical axis of rotation is different from the one that would be a limiting case of the orientations described above. In the above discussion, a 90-degree axis is vertical and the panels are rotating around the length of this axis. The vertical axis type of tracker being discussed in this paragraph rotates around a point, instead of a line. It is like placing the solar panel on the top of a vertical pole stuck in the ground. The axis of rotation is perpendicular to a horizontal surface and the surface of the solar panel can be tilted relative to this rotational axis. In vertical axis tracking, the surface azimuthal angle of the panel follows the sun's azimuthal angle. Only the azimuthal orientation of the panel is changing while the tilt of the panel remains unchanged. In general, vertical axis trackers have the panel tilted from the horizontal at an angle equal to the degrees of latitude of its location. As the latitude approaches the equator the panel tilt approaches zero degrees. As the panel becomes horizontal the effectiveness of vertical axis tracking is reduced. For this reason, vertical axis tracking is only used at higher latitudes [4].

1.2.3. Fixed Panels

Fixed panels can be looked at as a limiting case of tracking. Fixed solar panels can be considered a zero-axis tracker. The objective with a fixed panel is to orient the panel to optimize solar energy collection over a specified period of time. This specified period of time is usually one year, but other time periods can be used. The orientation of a solar panel is governed by two angles which are the tilt angle and the azimuthal angle as shown in Figure 1.2. The tilt angle is the angle between the ground and the surface of the panel, and the azimuthal angle is the angle between due south and a projection of the panel's surface normal onto a horizontal plane. It is the determination of these two angles that provide optimum energy incidence for clear sky and cloudy conditions that is the focus of this thesis work.

The object to which a fixed solar panel is mounted may limit the tilt and azimuthal angle of the installed solar panels. Two common objects to which solar panels are mounted are roofs and the ground. These different types of mounting achieve different goals; and what works for one application may not be viable for the other application. There are advantages and disadvantages of each mounting type.

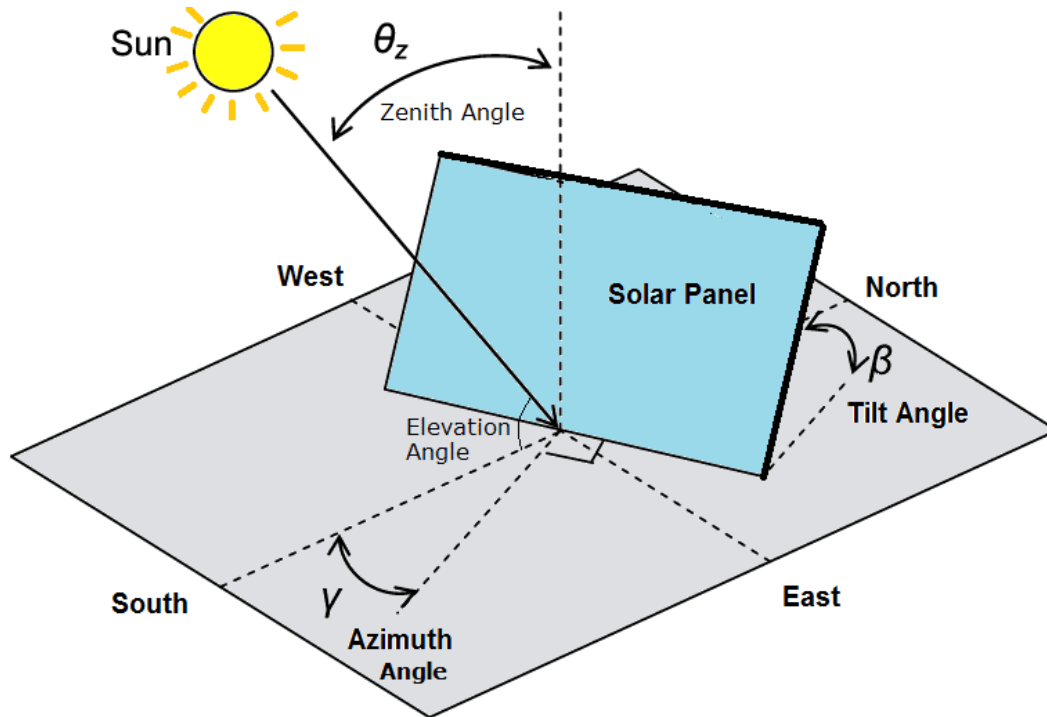


Figure 1.2: Schematic showing panel and sun angles [5].

1.2.3.1. Roof Mounted Solar Panels

Roof mount is the most common type of mounting technique for small scale applications of solar energy. This is especially true for home use, but also occurs for commercial buildings like Walmart stores. For this type of mounting, there is usually some type of racking attached to the roof and the solar panels are attached to the racking. A big advantage of roof mounting is that the solar panels use space that would normally go unused; and therefore, do not take up land that could be used for other activities. Typically, the installation costs of roof mounts are cheaper than that of ground mounts. The panels can also protect the roof from corroding elements in the atmosphere. Since, such panels are mounted on a roof, these panels can be protected from unauthorized usage. There are a few disadvantages to roof mounted solar panels. The biggest disadvantage is the limits placed on the orientation of the solar panels. Roofs that are orientated with azimuthal angles different than optimum, limit solar energy collection per unit area of panel. Tilt angles for the solar panels usually correspond to that of the roof and this also limits solar energy collection. Other disadvantages of roof mount solar panels are slanted roofs can be a safety

hazard for the installation team, solar panels covering the roof can make it more difficult to perform roof maintenance, and solar panels add weight to the roof.

1.2.3.2. Ground Mounted Solar Panels

A ground mount is when a solar panel is attached to the ground with the help of a frame structure made of steel or other type of material. They can be installed anywhere there is open space, and the conditions are suitable for solar energy collection. This makes them a great alternative to someone who does not have enough usable roof space or for those who do not prefer panels on their roofs. Placing solar panels on the ground is the only practical choice for large solar power plant installations. Ground mounting is more flexible than roof mounting as the roof may not be oriented towards the sun which would lead to a loss of overall energy production. Maintenance of panels is easier as you do not need to find your way around a sloping roof. Also, room for expansion is not an issue when it comes to ground mounted panels. Installation costs of ground mounted panels are usually higher than that of roof mounted panels because of the extra framing required. They also use up vast amounts of land which could be used for other applications. In addition, ground mounted panels are more susceptible to damage than roof mounted panels.

1.2.3.3. Fixed Panels versus Two and One-Axis Trackers

The way to collect the maximum solar energy with a given area of solar panel is to have the solar panel track both the east-west and altitude motions of the sun. This type of tracking is an expensive. Fixed mounting is the least expensive alternative in terms of capital costs, but captures the least amount of energy over a given time period. In between these two options, in terms of both capital cost and energy collection, are single-axis trackers. Compared to a fixed panel, a single or dual axis tracking panel will increase energy production by about 15-30% [6].

One and two-axis tracking systems require additional maintenance over fixed panels, which can be significant over a life span of 30 years. Common maintenance issues include the motors and other moving parts which are not required in a fixed panel system. This can increase the operation costs of two and one-axis tracking systems by 10 to 15% over fixed panels [6].

The topography of the location also has an impact on one-axis tracking systems. One-axis trackers are generally used for long strings of solar panels. For this reason, they require fairly level

ground. Sites with slopes or uneven terrain need substantial grading which adds cost to the installation. Soil conditions also need to be considered. Solar panels with one and two-axis tracking systems add extra torque to the metallic racks used to hold the panel. This means deeper piers need to be installed. Also, sites with poor soil conditions, like landfills, may not be open to installing trackers, as local laws would prevent disturbances below the surface. Rarely do you find two or one-axis trackers for roof mounted solar panels. These trackers add extra weight and torque to the roof, which is not desirable.

Another issue with two and one-axis trackers that should be discussed is their ability to handle winds. Most trackers are designed to withstand winds up to a certain velocity, but if the wind speed goes beyond this limit, the panels are stowed in a horizontal position. This protects the tracking mechanisms, but limits energy production during periods of high winds. This attribute of two and one-axis trackers limits their use to areas where wind speeds are generally low during the day.

At this time, fixed panels are the most commonly installed systems as they are more cost-effective and require the least maintenance. The additional energy produced by two and one-axis trackers does not outweigh these savings and the other advantages of fixed panels mentioned above. It is felt that the primary driver that has limited the use of two and one-axis tracking mechanisms with photovoltaic panels, is the low cost of photovoltaic panels. Between 1977 and 2015 the cost of solar panels has dropped by a factor of 253 [7]. This is an exponential price curve and it appears the trend will continue. Thus, solar installers tend to prefer using more panels to reach a desired energy production, as opposed to the higher energy capture obtained with two and one-axis trackers.

For these reasons, it is important to determine the optimum orientation of fixed solar panels. This needs to be done under a number of sky conditions and for a number of different time periods. By determining the optimum orientation of a fixed panel, we can increase energy production per unit area of solar panel and decrease the cost of electricity production with solar energy.

1.3. Optimum Solar Panel Orientation Work Done at Wright State

Over the past few years, four research projects studying optimum tilt angles have been conducted at Wright State University by graduate students. There have been two independent study

projects and two Master's thesis projects. The independent study projects were done by Nakrani [8] and Medarapu [9]. These two investigations used a Wright State developed code called Solar_PVHFC which was written by Gustafson [10]. The Master's thesis projects were done by Gugale [11] and Alhaidari [12]. The optimum panel orientation work presented in this thesis builds off of the work of Alhaidari [12].

Solar_PVHFC is a detailed computer model that determines the energy output of solar photovoltaic panels working in conjunction with hydrogen fuel cells and hydrogen tank storage. The only portion of Solar_PVHFC applicable to the work of Nakrani [8] and Medarapu [9] is the determination of the solar energy impinging on a unit area of the solar panels. Solar_PVHFC makes this calculation using a sky model (solar radiation impingement model) developed by Perez [13] which determines the amount of solar energy impinging on a solar panel at a given location on the surface of the earth, with a given orientation, at a specified time. This is a comprehensive calculation that includes the effect of beam radiation, radiation affected by the atmosphere, and radiation affected by the ground. The effects of clouds are included in this model because typical mean year experimentally measured solar radiation impinging on a horizontal surface at a given location is required in a sky model. The data used in Solar_PVHFC came from the National Renewable Energy Lab [14]. Using experimental data limits the locations that can be studied and limits the ability to control the cloud cover. Both Nakrani [8] and Medarapu [9] limited their optimum panel orientation study to one location, Dayton Ohio (latitude = 39.83°N , longitude = 84.06°E). To perform calculations like Nakrani [8] and Medarapu [9] did over the entire earth's surface, would require extremely large amounts of experimental data. For many locations on the earth's surface this data does not exist or is not easily accessible. At the present time, this eliminates a researcher from doing these types of calculations for the entire world. The other drawback of doing optimum panel orientation studies using sky models is the amount of cloud cover cannot be controlled. There are advantages for understanding purposes in controlling the amount of cloud cover input to the model in a systematic way. This is done in this work.

To gain control over the fundamental parameters that control optimum panel orientation and to remove the dependence on large amounts of experimental data, Gugale [11] and Alhaidari [12] adapted techniques that did not depend on measured solar radiation impinging on a horizontal surface at a given location. This was done by using atmospheric transmissivity equations. These do require some experimental constants that depend on the atmospheric conditions present at a

given location, but there are relatively few of them and offer quantifiable control over the effect of the atmosphere. In making this step, a detailed description of the weather conditions at a given location are lost, but the freedom to perform optimum panel orientation calculations for the entire earth's surface is gained; as well as the ability to study the effect of cloud cover in a controllable, quantifiable manner.

In addition to removing the dependence on detailed experimental data, Gugale [11] and Alhaidari [12] developed algebraic expressions for the optimum tilt angle of the panel as a function of location and time. Prior to the work of Gugale [11], optimum tilt angle equations existed for the case of two-axis [15] and one-axis tracking [15] for beam radiation with no atmosphere. That is, the effects of the atmosphere and ground reflection are not included in these equations. Gugale [11] developed the algebraic expressions that include beam, diffuse (atmospheric effects), and ground reflected radiation. Note that Nakrani [8] and Medarapu [9] found optimum tilt angles by solving the sky model equations at many orientations of the panel and picking out the one that intercepted the most solar energy. This is an accurate way of performing this optimization, but a labor intensive process. This will be referred to as the brute force technique in this thesis. Gugale's [11] equations show the effect of changing beam, diffuse, and ground reflected transmissivities on optimum tilt angles in algebraic equation form. Gugale [11] greatly simplified the process of finding optimum tilt angles for two and one-axis tracking including the effects of the atmosphere and ground reflections.

Alhaidari [12] attacked the more difficult case of finding optimum tilt angles for fixed solar panels. Up until the time of Alhaidari [12], these calculations were done using the brute force method as done by Nakrani [8] and Medarapu [9] or using rules-of-thumb. The simplest rule-of-thumb, but the most used, is pointing fixed panels in the Northern Hemisphere due south and tilting them at an angle equal to the latitude where the panel is located. In the Southern Hemisphere the same tilt angle is used, but the azimuthal orientation is due north. Alhaidari [12] developed a detailed and precise equation for the optimum tilt of these solar panels for the case of no atmosphere and the case of clear atmosphere. The only approximation made by Alhaidari [12] was to ignore the change of sunrise and sunset on the panel with tilt angle. This assumption is removed in this work. The math becomes very complex when this is done, but it is desired to know the effect of ignoring this issue. Essentially the work of this thesis picks up where Alhaidari's [12] work leaves off.

1.4. Goals and Outline of Thesis

1.4.1. Literature Survey

In Chapter 2 of this thesis, the reader will be provided with a brief description of some of the literature published on optimum tilts of solar panels. The beginning of this literature survey was started in Chapter 1 and it provided the reader with the history of this work at Wright State and where the present thesis work fits into this progression. Chapter 2 extends the review of the Wright State work, and includes the broader published work done on optimum panel orientation. The optimum panel orientation studies presented in Chapter 2 are generally for a limited number of locations or a single location. The method used by Nakrani [8] and Medarapu [9], which have the best physical fidelity, is used, but does not allow for world-wide studies. The largest study that uses this brute force technique covers the continental United States and was done by Lave and Kleissl [16]. While this work is impressive, it does not appear to be expandable to the entire world due to a lack of experimental data. The work presented in this thesis and the work of Alhaidari [12] are the only publications to present optimum tilt angles for fixed solar panels over the entire surface of the earth. Gugale's [11] optimum tilt angle models for two and one-axis trackers have the capability to do this, but for moving panels these optimum tilt angles change for every hour of the year. This makes complete data presentation prohibitive. Thus, Gugale [11] only presented data for one latitude. When fixed panels are used, the time variable is integrated away, greatly reducing the amount of data that needs to be presented to fully describe optimum tilts for the entire world. Thus, Alhaidari [12] presented optimum tilt angles for the entire world, and this work does too.

1.4.2. Derivation of Clear Sky Optimum Tilt Equation

Because Alhaidari's [12] development of the optimum tilt of a fixed panel for a specified period of time, for no atmosphere and clear atmosphere cases ignored the change in sunrise and sunset on the panel with panel tilt, this work spends time including this effect in the derivation. A number of derivative of integral terms result when this is done. The clear sky equation to include this effect is rederived in Chapter 3 of this thesis. Including this effect greatly increases the complexity of the derivation and the resulting optimum panel tilt equation. This derivation is presented in detail so the reader can judge its validity and so a detailed understanding of the physics involved in optimum solar panel orientations can be seen in equation form.

1.4.3. Transmissivities that Include Cloud Effects

The more important achievement of this thesis work is the inclusion of the effects of cloud cover in a manner that the amount of cloud cover is an input to the analysis and the effects of cloud cover on optimum tilt angles can easily be seen and determined. To make this happen, equations for beam and diffuse transmissivities that are a function of the amount of cloud cover are required. Investigators who are known to have attempted this task are Kasten-Czeplak [17]. The equations of Kasten-Czeplak [17] alter beam and diffuse transmissivities for clear skies to get beam and diffuse transmissivities for cloudy skies. Because the clear sky beam and diffuse transmissivity models provided by Kasten-Czeplak's [17] result in physically unreasonable results close to sunrise and sunset, they are not used in this work. The alterations implemented in this work and their justification are given in Chapter 4. It is cloudy sky beam and diffuse transmittances that transform the clear sky model presented in Chapter 3, into a cloudy sky model.

1.4.4. Results for Entire World

Chapter 5 presents a complete set of optimum tilt angle results for the entire world, for all azimuthal angles, for a one-year time period, for varying degrees of cloud cover. The range of cloud cover addressed runs from no clouds, clear sky, to complete cloud cover. The azimuthal angle is taken as a parameter in these studies, but the yearly energy incident on a unit area of panel provides the information from which the optimum azimuthal angle can be obtained. In general, the optimum azimuthal angle is due south for the northern hemisphere, and due north for the southern hemisphere. The first results presented in Chapter 5 are for unvarying cloud cover over the entire year. The second set of results is where the cloud cover takes on one value for six months of the year and a different value for the remaining 6 months of the year. This was done to mimic changing cloud cover as a function of season. The third set of results looks at different cloud cover in the morning as compared to the afternoon. No changes are made from day to day, just from morning to afternoon. This set of results is intended to give the reader an understanding of the effects of changing cloud cover over the course of a day. These cloud cover scenarios are not meant to replicate a specific cloud cover at a specific location, but to provide the reader with information on how cloud cover affects optimum tilt angles and the amount of solar energy incident on a solar panel over a yearly time period. While the model is capable of using any desired period, only yearly results are presented in this thesis.

1.4.5. Conclusions

To close this thesis, a summary of important conclusions and aspects of this work are made in Chapter 6. A couple of recommendations on future work are also given.

Chapter 2

Connections to Others Work

This chapter provides an overview of others work that has some relationship to the work being presented in this thesis. The hope is to provide the reader with some perspective on this thesis work and how it fits into the broader work done on optimum panel tilts and calculating solar radiation incident on a tilted surface. This literature survey is not meant to be comprehensive, but designed to give the reader a feel for other work done in the field. Since determining the amount of radiation on a titled surface is critical to the work of optimum panel tilts, the first section of this chapter presents a number of sky models available for doing this. In this work, the isotropic sky model of Liu and Jordan [18] is used, but other choices could have been made. The second section of this chapter deals with another aspect that is important to this work; atmospheric transmissivity models. The third section of this chapter presents some of the work that has been done determining optimum tilts of solar panels. Lastly, some specifics from the work done at Wright State University in the area of optimum panel tilts is presented. This thesis work rests on the Wright State researchers of the past.

2.1. Sky Models

Sky models are used to determine the amount of solar radiation impinging on a titled panel located on the surface of the earth. This is done based on knowledge of the total solar impinging on a horizontal surface. One may wonder why the term “sky” is used for a model that takes the solar energy flux on a horizontal surface and translates it to a surface of different tilt and some

azimuthal orientation when the tilted surface and the horizontal surface are at the same location? One might say this does not include the effects of the sky, or stated a different way, this does not include the effects of the atmosphere. Sky models do indeed include the effects of the atmosphere. In a sky model, the total solar energy flux on a horizontal surface must be split into beam and diffuse components; it is the atmosphere that dictates this split. In addition, it is the atmosphere that dictates the magnitude of the given total solar insolation on a horizontal surface. Thus, the name sky model is appropriate for a model that uses the total insolation on a horizontal surface and translates it to a surface of some other orientation.

There are three basic components of solar radiation included in a sky model. The first of these is the beam radiation. The beam radiation is the component of solar radiation that reaches the earth's surface without interaction with the atmosphere. The second basic component is called the diffuse radiation. Diffuse radiation is radiation that has been scattered off the atmosphere and reaches the surface of the earth. The third basic component is ground reflected radiation. Ground reflected radiation is the beam and diffuse radiation that hits the ground and is reflected. Isotropic sky models deal with these three components in their totality, while anisotropic sky models break the diffuse component into two or three subcomponents. These three subcomponents would be isotropic, circumsolar, and horizon brightening. Isotropic diffuse has the same intensity in every direction, while circumsolar and horizon brightening have preferential scattering directions. Circumsolar is forward scattering of the solar radiation as it travels through the atmosphere and horizon brightening is preferential scattering from the horizon.

A tabulation of some of the sky model variants is shown in Table 2.1. All these models are written in terms I 's which is the solar energy falling on a horizontal unit area in a one-hour time period. The first sky model shown in this table is that of Liu and Jordan [18]. This is the sky model used in this work. In looking at the Koronokis [19], Badescu [20], and the Tian et al. [21] isotropic sky models, it can be seen that the only difference from the Liu and Jordan model is the view factor on the diffuse radiation term. The diffuse radiation view factor in the Liu and Jordan model is $\left(\frac{1+\cos\beta}{2}\right)$, while that on the other three isotropic models is the factor in parenthesis just after I_D . The Liu-Jordan model is preferred in this work because the view factor for the ground reflected radiation, $\left(\frac{1-\cos\beta}{2}\right)$, plus that for the diffuse radiation, $\left(\frac{1+\cos\beta}{2}\right)$, add to one. From a purely geometric perspective, this has to be. The anisotropic models presented in Table 2.1 are those of

Hay and Davis [22], Reindl [23], Hay, Davis, Reindl and Klucher [22]. The Hay and Davis model divides the diffuse radiation into circumsolar and isotropic diffuse. This is done with the factor A_c in the equation; this adds the circumsolar part to the beam radiation and subtracts it from the diffuse isotropic term. The anisotropic models of Reindl [23] and Hay, Davis, Reindl and Klucher [22] separately address all three components of the diffuse radiation.

Table 2.1: Some models that have been used to determine the amount of solar insolation on a tilted surface including the effects of the atmosphere.

Researchers	Type	Total Insolation on a Tilted Surface
Liu and Jordan [18]	Isotropic	$I_T = I_b R_b + I_g \rho \left(\frac{1 - \cos \beta}{2} \right) + I_d \left(\frac{1 + \cos \beta}{2} \right)$
Koronokis [19]	Isotropic	$I_T = I_b R_b + I_g \rho \left(\frac{1 - \cos \beta}{2} \right) + I_d \left(\frac{2 + \cos \beta}{3} \right)$
Badescu [20]	Isotropic	$I_T = I_b R_b + I_g \rho \left(\frac{1 - \cos \beta}{2} \right) + I_d \left(\frac{3 + \cos 2\beta}{4} \right)$
Tian et al. [21]	Isotropic	$I_T = I_b R_b + I_g \rho \left(\frac{1 - \cos \beta}{2} \right) + I_d \left(1 - \frac{\beta}{180} \right)$
Hay and Davis [22]	Anisotropic	$I_T = (I_b + I_d A_c) R_b + I_g \rho \left(\frac{1 - \cos \beta}{2} \right) + I_d \left(\frac{1 + \cos \beta}{2} \right) (1 - A_c)$
Reindl [23]	Anisotropic	$I_T = (I_b + I_d A_c) R_b + I_g \rho \left(\frac{1 - \cos \beta}{2} \right) + I_d \left(\frac{1 + \cos \beta}{2} \right) (1 - A_c) \left[1 + \sqrt{\frac{I_b}{I_g}} \sin^3 \frac{\beta}{2} \right]$
Hay, Davis, Reindl and Klucher [22]	Anisotropic	$I_T = (I_b + I_d A_c) R_b + I_g \rho \left(\frac{1 - \cos \beta}{2} \right) + I_d \left(\frac{1 + \cos \beta}{2} \right) (1 - A_c) \left[1 + \sin^3 \frac{\beta}{2} \right]$

2.2. Transmissivity Models

The purpose of transmissivity models is to obtain the beam and diffuse radiation falling on a horizontal unit area located on the surface of the earth from the solar radiation just above the atmosphere. The two quantities produced by these models are the beam transmissivity and the diffuse transmissivity. Two categories of these transmissivities are recognized, clear sky transmissivities and cloudy sky transmissivities.

2.2.1. Clear Sky Transmissivity Models

Some of the models that provide beam transmissivities for clear sky conditions are shown in Table 2.2 and models that provide diffuse transmissivities for clear sky conditions are shown in Table 2.3. It is easier to find models for clear sky beam transmissivities, than clear sky diffuse transmissivities.

Table 2.2: Some beam transmissivity models.

Researchers or Model Name	Beam Transmittance Model
Hottel [24]	$\tau_{b,cs} = a_0 + a_1 e^{\left(\frac{-k}{\cos\theta_z}\right)}$
ASHRAE [25]	$\tau_{b,cs} = \frac{A}{I_{on}} e^{\left(\frac{-B}{\cos\theta_z}\right)}$
Heliosat-1 Model [26]	$\tau_{b,cs} = e^{(-m_{air}\sigma_{TLTF})}$
Haurwitz [27]	$\tau_{b,cs} = \cos\theta_z e^{\left(\frac{-0.057}{\cos\theta_z}\right)}$
Robeldo and Sole [28]	$\tau_{b,cs} = (\cos\theta_z)^{1.179} e^{(-0.0019(90-\theta_z))}$
Berger and Duffie [28]	$\tau_{b,cs} = 0.7\cos\theta_z$
Adnot et al. [28]	$\tau_{b,cs} = (\cos\theta_z)^{1.15}$
Meinel [29]	$\tau_{b,cs} = 0.7m_{air}^{0.678}$
Kasten and Czeplak [17]	$\tau_{b,cs} = 0.47 - \frac{0.016}{\cos\theta_z}$

Table 2.3: Some diffuse transmissivity models.

Researchers or Model Name	Diffuse Transmittance Model
Lui and Jordan [18]	$\tau_{d,cs} = 0.271 - 0.294\tau_{b,cs}$
Kasten and Czeplak [17]	$\tau_{d,cs} = 0.43\tau_{b,cs}$
Erbs et al. [30]	$\tau_{d,cs} = 0.198\tau_{b,cs}$ for $\tau_{b,cs} > 0.67$
Orgill and Hollands [31]	$\tau_{d,cs} = 0.215\tau_{b,cs}$ for $\tau_{b,cs} > 0.62$
Carroll [32]	$\tau_{d,cs} = -0.0586 - \tau_{b,cs} + \sqrt{0.00343 + 0.976\tau_{b,cs}}$

The beam transmissivity models shown in Table 2.2 are of two basic types, those that have the zenith angle of the sun in an exponential function and those that do not have the zenith angle inside an exponential function. Some of the equations do not show a zenith angle directly, but it is buried inside the air mass parameter, m_{air} . There are a number of parameters and constants in

these equations that are not defined here. The reader will have to consult the reference sources to obtain this information. It should also be stated that a number of these equations were meant for a specific location on the surface of the earth, and numbers in these equations may change somewhat for different locations. Again, the original sources should be consulted. The purpose of this table is to provide the reader with some sense of the forms of these equations. More complex models of the beam transmissivity exist, such as the Bird model [33] and its variants, and they keep the exponential functional dependence on the zenith angle. Good surveys of beam transmittance models can be found in Al Aboosi [34] and Bird and Hulstrom [35]. The beam transmissivity model used in this work is that of Hottel [24] and it is the first one listed in Table 2.2.

The diffuse transmissivity models given in Table 2.3 are of three types. The first type is the Liu and Jordan model [18] that has the diffuse transmissivity decreasing from an upper limit of 0.271 as the beam transmissivity increases. The second type is illustrated by the models of Kasten and Czeplak [17], Erbs et al. [30], and Orgill and Hollands [31]. These models show the diffuse transmissivity increasing as the beam transmissivity increases. This is not believed to be the best way to model diffuse transmissivities, as will be discussed in Chapter 4. The models of Kasten and Czeplak [17], Erbs et al. [30], and Orgill and Hollands [31] are clear sky limits of cloudy sky models and these researchers have not explicitly recommended their models for clear sky situations. The last model shown in Table 2.2 has a more complex dependence on the beam transmissivity. In this model the beam transmissivity increases and then decreases as a function of the beam transmissivity. The increase occurs between beam transmittances of 0 to 0.2 and then the diffuse transmissivity becomes a decreasing function.

2.2.2. Cloudy Sky Transmissivity Models

Determining beam and diffuse transmissivities under the effects of clouds is a difficult task for two reasons. The first reason is the amount of cloud cover is whether dependent and is hard to quantify for any given location, for any given time. The second reason handling cloud cover is difficult is cloud type affects the amount of solar radiation reaching the earth's surface. The best way to model cloud cover is to use some solar radiation measurement that quantifies the cloud cover at a given location, at a specified time in a statistical manner. Such a typical parameter would be the global solar radiation impinging on a horizontal surface. When this measured parameter is compared to the global solar radiation on a horizontal surface just above the atmosphere, the effects

of the atmosphere and clouds can be ascertained. Global solar radiation on a horizontal surface has been measured for a number of locations around the world on an hourly basis. Cloudy sky models that use measured global solar irradiation on a horizontal surface can be referred to as decomposition models, because they separate the measured global solar radiation into a beam and diffuse component using a mathematical model. Haurwitz [27], Erbs et al. [30], and Orgill and Hollands [31] have published decomposition techniques. A second technique for calculating beam and diffuse transmissivities under cloudy conditions uses a parameter that specifies the fraction of cloud cover at a certain location, for a certain time. While these cloud cover fractions can be based on measured data, these fractions allow a user to control the amount of cloud cover easily. For parametric studies, such as done in this thesis, this is helpful. The cloud cover models of Robinson [36] and Kasten and Czeplak [17] are of this type. In this work the cloud cover model of Kasten and Czeplak [17] is used with some modifications. The model and the alterations made to this model are described in detail, in Chapter 4. The cloud cover model developed by Kasten and Czeplak [17] is based on analyzing cloud data over a 10-year period. Many studies have been done by researchers on the Kasten and Czeplak model [17] and they have found the results to be reasonable using the original coefficients in the equation; better results are obtained using site specific coefficients. Using locally fitted coefficients Ahamed, Guo and Tanino [37] show good results for four cities in Western Canada.

2.3. Optimum Tilt Studies around the World

There has been a lot of research done over the years which determines the optimum tilt of a solar panel for specific locations. Some of these will be discussed in this section.

This has been done for annual, seasonal, and monthly time periods by Karkee et al. [38] for five different cities in Nepal; namely, Kathmandu, Biratnagar, Pokhara, Jumla and Mahendranagar. The results from Karkee et al. are shown in Table 2.4. It is obvious from these results that the optimum tilt angle is steeper in the winter when the sun is low in the sky and shallower in the summer when the sun is high in the sky. For a yearly period, the optimum tilt angle is close to that of the latitude. There is a rule-of-thumb in the solar field that says this should be the case if atmospheric effects are ignored [39] [15]. Clouds will affect these results if they occur preferentially at certain times of the year.

Table 2.5 shows the optimum tilt results of 8 more sets of investigators. Most of these investigations are for a one-year time period, but some have time periods of one month and one has a time period of the summer season. Some of these investigations were performed experimentally and some were performed computationally. All of these investigations are in the northern hemisphere and have the solar panels pointing due south. For the most part, these investigators have done experiments or calculations for one or two sites only, and they include the effects of the local weather.

The monthly results of Jafarkazemi and Saadabadi [40], Kacira et al. [41], and Ahmad and Tiwari [42] all follow the trends of the results of Karkee et al. [38] shown in Table 2.4. The winter months, when the sun is low in the sky, have tilt angles greater than the latitude and the summer months, when the sun is high in the sky, have tilt angles lower than the latitude. These differences between the winter and summer are significant and this is why Calabro [43] and Jafarkazemi and Saadabadi [40] discuss using two different tilt angles over the course of a year. This would slightly increase the operating costs involved in running a solar farm, but more solar energy could be collected. Kacira et al. [41] indicate the gains in the amount of solar radiation received by the panel comparing monthly varying tilt to a seasonally varying tilt and to a tilt equal to the latitude as being 1.1% and 3.9% respectively.

Table 2.4: Karkee et al's. [38] optimum tilt angle results for different periods of the year.

Location	Latitude	Yearly Optimal Tilt	Winter Optimal Tilt	Summer Optimal Tilt	Maximum Monthly Optimal Tilt	Minimum Monthly Optimal Tilt
Kathmandu	27.72°	32°	50°	4°	59° (December)	0° (May, June, July)
Pokhara	28.21°	32°	51°	4°	60° (December)	0° (May, June, July)
Biratnagar	26.45°	30°	48°	2°	58° (December)	0° (May, June, July)
Mahendranagar	28.99°	31°	50°	5°	60° (December)	0° (May, June, July)
Jumla	29.28°	32°	52°	5°	61° (December)	0° (May, June, July)

The summer season computational results of Calabro [43] using data of daily global solar radiation collected by the Italian institute of ENEA are also given in Table 2.5. Calabro's [43] study was done for northern latitude angles of 36° to 46°. In all of Calabro's [43] studies, the optimum panel tilt was 26° to 28° less than the latitude angle. This is reasonable for the summer season when the sun is high in the sky.

The yearly results of Jafarkazemi and Saadabadi [40], Jamil et al. [44], Kern and Harris [45], and Ahmad and Tiwari [42] all have optimum tilt angles that are within 2° of the latitude where the panels are located. Optimum tilt angles from the work of Soleimani et al. [46] and Raptis et al. [47] differ by approximately 13° and 8° degrees, respectively. It may be that the optimum tilt reported by Soleimani et al. [46] is somewhere between 23° and 29°, because the experimental resolution of their data points was 0, 23, 29, 35 and 42°. Raptis et al. [47] also experimentally determined a yearly optimum panel tilt. Their optimum tilt was found to be 30° for a latitude

Table 2.5: Yearly optimum tilt angle results for several locations.

Investigators	Location	Latitudes	Time Period	Optimum Tilt
Jafarkazemi and Saadabadi [40]	Abu Dhabi	24.4 °	Monthly	9° to 52° from Summer Winter
Kacira et al. [41]	Sanliurfa, Turkey	37.17°	Monthly	13° in June 61° in December
Ahmad and Tiwari [37]	New Delhi, India	28.61°	Monthly	58° in December 0° in July
Calabro [43]	Northern Latitudes	36° to 46°	Summer	26° to 28° less than latitude
Jafarkazemi and Saadabadi [40]	Abu Dhabi	24.4 °	Yearly	22°
Soleimani et al. [46]	Tehran, Iran	35.7°	Yearly	23°
Jamil et al. [44]	Aligarh, India	27.9°	Yearly	27.6
Jamil et al. [44]	New Delhi, India	28.6°	Yearly	28.0
Ahmad and Tiwari [42]	New Delhi, India	28.61°	Yearly	30°
Raptis et al. [47]	Athens, Greece	37.98°	Yearly	30°

location of 37.98° . Raptis et al. [47] indicate that this lower optimum tilt angle was due to clouds in the winter. Clouds in the winter skew the tilt to shallower angles so more solar energy is collected in the summer when the clouds are not prevalent.

2.4. Research Done at Wright State University

Both Nakrani [8] and Medarapu [9] carried out studies of optimum tilt angles for Dayton, Ohio (39.83°N latitude, 84.06°E longitude) using typical meteorological year data from the National Renewable Energy Lab [48]. This data includes typical weather conditions, including cloud cover. As mentioned in Chapter 1, both of these studies used the brute force method of determining optimum tilt angles which meant energy impingement was calculated for many orientations, and the orientation with the highest incident energy was taken as the optimum. This is a time-consuming process and resolution of results is limited to the angle increment used in each of these studies which is 5° . While Nakrani and Medarapu studied many types of solar tracking systems, it can be said that Nakrani focussed on fixed solar panels and Medarapu focused on one-axis tracking systems.

Results for some of the fixed solar panel cases simulated by Nakrani [8] and the vertical-axis tracking cases simulated by Medarapu [9] are tabulated in Table 2.6. This table provides the optimum tilt angle and the optimum azimuthal angle found by these investigators. For the vertical-axis tracking system the azimuthal angle follows the azimuthal angle of the sun and is marked as ‘varies’ in Table 2.6. For both types of solar panels, results are presented on a seasonal and yearly basis. For fixed panels, results have been produced that optimize energy collection during the evening hours when homeowners have returned from work. The “>” in Table 2.6 means the investigator did not check higher angles and the optimum angle and energy capture may be larger than the values shown in the table.

For all cases in Table 2.6, the optimum tilt angles are higher for winter than summer with spring and fall values between these. The fall optimum tilt angles are generally steeper than those in the spring. Energy collection follows the same trends as the optimum tilt angles. All seasons are taken as three months and have approximately the same number of days. Yearly energy collection is close to the summation of the seasonal values, but not exactly the same. Optimizing panel orientation for each individual season provides slightly more energy than using a single optimum tilt angle for all seasons. While the optimum azimuthal angle is due south for all fixed panel cases

that cover an entire day, fixed panel cases that focus on evening power generation have azimuthal angles that point to the west.

Table 2.6: Selected optimum tilt angle results of Nakrani [8] and Medarapu [9] for Dayton, Ohio (39.83°N latitude, 84.06°E longitude). Note that positive azimuthal angles point west.

Investigator	Tracking Type	Season	Portion of Day	Optimum Tilt	Optimum Azimuthal Angle	Energy at Optimum Tilt (kW-h/m ²)
Nakrani [8]	Fixed	Winter	Full	>55°	0°	>237
Nakrani [8]	Fixed	Spring	Full	30°	0°	427
Nakrani [8]	Fixed	Summer	Full	25°	0°	511
Nakrani [8]	Fixed	Fall	Full	45°	0°	368
Nakrani [8]	Fixed	Yearly	Full	35°	0°	1500
Nakrani [8]	Fixed	Winter	Evening	>55°	55°	>177
Nakrani [8]	Fixed	Summer	Evening	>55°	85°	>249
Nakrani [8]	Fixed	Yearly	Evening	>55°	75°	>935
Medarapu [9]	One-Axis Vertical	Winter	Full	60°	varies	267
Medarapu [9]	One-Axis Vertical	Spring	Full	45°	varies	526
Medarapu [9]	One-Axis Vertical	Summer	Full	40°	varies	634
Medarapu [9]	One-Axis Vertical	Fall	Full	55°	varies	442
Medarapu [9]	One-Axis Vertical	Yearly	Full	50°	varies	1856

Gugale's [11] and Alhaidari's [12] research at Wright State University involved developing clear sky models for optimum tilt angles of solar panels. Gugale developed a model for two and one-axis tracking panels that provides optimization at a moment in time and Alhaidari developed a model for fixed solar panels over a specified time period. Gugale's work was easier than Alhaidari's because difficult integrations over time had to be performed by Alhaidari. This is one reason why Gugale's work was a precursor to Alhaidari's work.

Starting from the isotropic sky model for the amount of solar radiation on a surface, Gurgale [11] developed the equation

$$\tan \beta = \tan \theta_z \frac{\cos(\gamma_s - \gamma)}{\frac{\tau_d}{2\tau_b} - \rho_g \frac{\tau_d}{2\tau_b} - \frac{\rho_g}{2} + 1} \quad (2.1)$$

to determine the optimum tilt, β , of a solar panel at a given instant as a function of the position of the sun in the sky, θ_z and γ_s , the azimuthal orientation of the solar panel, γ , and atmosphere and surface conditions, τ_b , τ_d , and ρ_g . The factor

$$\frac{1}{\frac{\tau_d}{2\tau_b} - \rho_g \frac{\tau_d}{2\tau_b} - \frac{\rho_g}{2} + 1} \quad (2.2)$$

is simply an adjustment to the no atmosphere optimum tilt angle to include the effects of the atmosphere. The shortcoming of Equation (2.1) is that it cannot be used for fixed panels over a finite period of time. Alhaidari [12] has addressed this issue.

For fixed solar panels, Alhaidari [12] developed the equation,

$$\tan \beta = \tan^{-1} \frac{A}{B}. \quad (2.3)$$

where,

$$\begin{aligned} A = & -\cos\phi\cos\gamma \sum_{n=1}^{365} \int_{t_{sr}}^{t_{ss}} G_{on}\tau_b \sin\delta dt_d \\ & + \sin\phi\cos\gamma \sum_{n=1}^{365} \int_{t_{sr}}^{t_{ss}} G_{on}\tau_b \cos\delta \cos\omega dt_d \\ & + \sin\gamma \sum_{n=1}^{365} \int_{t_{sr}}^{t_{ss}} G_{on}\tau_b \cos\delta \sin\omega dt_d \end{aligned} \quad (2.4)$$

and

$$\begin{aligned} B = & \sin\phi \sum_{n=1}^{365} \int_{t_{sr}}^{t_{ss}} G_{on}\tau_b \sin\delta dt_d \\ & + \cos\phi \sum_{n=1}^{365} \int_{t_{sr}}^{t_{ss}} G_{on}\tau_b \cos\delta \cos\omega dt_d \\ & + 0.5 \sum_{n=1}^{365} \int_{t_{sre}}^{t_{sse}} G_{on} \cos\theta_z \tau_d dt_d \\ & - 0.5\rho \sum_{n=1}^{365} \int_{t_{sre}}^{t_{sse}} G_{on} \cos\theta_z (\tau_b + \tau_d) dt_d \end{aligned} \quad (2.5)$$

to determine the optimum tilt angle over a finite period of one year. It is easily seen that this equation is more complex than the equation developed Gugale [11]. The summations in this equation are over all days in a year and the integrals go from sunrise to sunset for each day in the year. It will be seen in Chapter 3 that this is a simplified version of the equation developed in this thesis. Essentially the models developed at Wright State are becoming more complex as new theses are undertaken.

Chapter 3

Derivation of Optimum Tilt Equation

In this chapter trigonometric, integral equations will be derived to find the optimum tilt angle of a fixed solar panel as a function of location on the surface of the earth for a finite period of time. The azimuthal angular orientation of the panel is taken as a parameter in this development and the optimum tilt angle is found as a function of this quantity. Other parameters in the equation are the ground reflectivity, the beam transmittance, and the diffuse transmittance. The beam and diffuse transmittances can be adjusted to produce results for no-atmosphere conditions, clear atmosphere conditions, and cloudy atmosphere conditions. The focus of this thesis is cloudy atmospheric conditions, but clear atmospheric conditions will be presented as a limiting case of cloudy conditions.

Much of the derivation presented here follows the work of Alhadari [12], except for the inclusion of the change of sunrise and sunset on the panel as a function of the tilt angle of the panel. Including this effect is a substantial amount of work, as you will see in the second and third sections of this chapter. The first section below provides the equation for the solar radiation incident on the panel as a function of time, location, and orientation of the panel. This material is only an altered presentation of the work done by Alhadari [12]. In the second section, where the derivative of the equation developed in the first section is taken, differences occur. Since the third section is finding the rate of change of sunrise and sunset on the panel as a function of the panel tilt angle this development is unique to this thesis.

3.1. Solar Incidence Energy

The starting point for this derivation is the equation for the amount of solar energy impinging on a panel as a function of location on the surface of the earth, orientation of the panel (both tilt and azimuthal angles), and the time of the day and year. This is essentially a sky model. For this work the isotropic sky model put forth by Liu and Jordan [49] is used,

$$G_T = G_b R_b + G_d \left(\frac{1 + \cos \beta}{2} \right) + G \rho \left(\frac{1 - \cos \beta}{2} \right). \quad (3.1)$$

This equation includes beam, atmospheric diffuse, and ground reflected components of solar energy hitting the surface of the panel. The first term on the right-hand side of this equation accounts for beam radiation, the second term accounts for diffuse radiation scattered off of the atmosphere, and the third term accounts for diffuse radiation reflected off the ground around the solar panel. Whereas the isotropic sky model is generally written in terms of hourly solar energies impinging on a unit area [15], the isotropic sky model presented in Equation (3.1) is written in terms of solar radiative powers impinging on a unit area of panel. This change was made because of the time integrations that have to be carried out in this work. All the G terms in Equation (3.1) are radiative fluxes: G_b is the beam radiation falling on a horizontal surface, G_d is the atmospheric diffuse radiation falling on a horizontal surface, G is the total radiant energy falling on a horizontal surface, and G_T is the total solar radiation falling on the tilted panel surface. The total radiation on a horizontal surface is simply the sum of the beam and diffuse components on a horizontal surface,

$$G = G_b + G_d. \quad (3.2)$$

The R_b in Equation (3.1) is the ratio of beam radiation on a tilted surface to that on a horizontal surface,

$$R_b = \frac{\cos \theta}{\cos \theta_z}, \quad (3.3)$$

where θ is the incident angle of the beam radiation on the panel and θ_z is the zenith angle of the sun in the. Both of these angles vary over the course of a day and over the course of a year. The remaining quantities in Equation (3.1) are ρ which is the ground reflectivity and β which is the tilt angle of the panel from the horizontal.

The goal of the derivation presented in the next two sections of this chapter is to optimize G_T as a function of β . This is more complicated than it initially seems because the incident angle of the beam radiation on the surface of the panel, θ , is a complex function of β and many of the

quantities in Equation (3.1) are a function of time. Remember the goal is to optimize G_T for a period of time, like one year.

Expressions for the cosine of the incident angle and the cosine of the zenith angle can be found in many solar energy textbooks, for example *Solar Engineering of Thermal Processes* by Duffie and Beckman [15] provides these equations. The incident angle equation is

$$\begin{aligned} \cos\theta = & \sin\delta\sin\phi\cos\beta - \sin\delta\cos\phi\sin\beta\cos\gamma + \cos\delta\cos\phi\cos\beta\cos\omega \\ & + \cos\delta\sin\phi\sin\beta\cos\gamma\cos\omega + \cos\delta\sin\beta\sin\gamma\sin\omega, \end{aligned} \quad (3.4)$$

where the angles γ , ϕ , δ , ω , and β are the azimuthal angle of the panel, the latitude of the location of the solar panel, the declination angle of the earth's axis of rotation, the hour angle of the position of the sun in the sky over the course of a day, and the tilt angle of the panel. These are standard sun-earth angles that can be found in solar energy textbooks [15]. The latitude specifies the location of the panel and is simply an input to this analysis, whereas the declination and hour angles are time dependent angles. The declination angle is given by,

$$\delta = 23.45\sin\left(360\frac{284 + n_d}{365}\right). \quad (3.5)$$

and the hour angle is,

$$\omega = 15(t_d - 12). \quad (3.6)$$

In these equations the quantity n_d represents the day of the year counted from January 1 and t_d the hour of the day in military, solar time counted from midnight, where midnight is taken as the beginning of the 24-hour day, not the end of the day. Note that fractions of days and fractions of hours are allowed in these equations. In Equation (3.6) the number 15 dictates that the hour angle is given in degrees and the number 12 dictates that the time of day since midnight is given in hours. The cosine of the zenith angle is determined from,

$$\cos\theta_z = \cos\delta\cos\omega\cos\phi + \sin\delta\sin\phi. \quad (3.7)$$

Like the incidence angle given in Equation (3.4), it can be seen that the zenith angle is written in terms of some standard angles used in the solar energy discipline.

The standard way to solve Equation (3.1) is to use experimental measurements of G as a function of time for a given location. G is separated into G_b and G_d using Equation (3.2) and the clearness index,

$$k = \frac{G}{G_{on}\cos\theta_z}, \quad (3.8)$$

where G_{on} is the extra-terrestrial solar radiation normal to the sun's rays just above the earth's atmosphere,

$$G_{on} = G_{sc} \left(1 + 0.033 \cos \frac{360n_d}{365} \right). \quad (3.9)$$

As mentioned before, the difficulties with this technique are obtaining the required experimental data for G , for all locations of interest and controlling the cloud cover in a quantitative manner so that the effects of clouds on the optimum tilt angle can be deduced.

In this work, the quantities G_b and G_d are obtained from beam, τ_b , and diffuse, τ_d , atmospheric transmissivities. Equations for τ_b and τ_d based on a few constants will be given in Chapter 4. Neither τ_b or τ_d are a function of the panel tilt angle, but they are a function of the panel location and the time through Equation (3.7). The beam radiation on a horizontal surface that goes into Equation (3.1) is,

$$G_b = G_{on} \tau_b \cos \theta_z; \quad (3.10)$$

and the diffuse radiation on a horizontal surface that goes into Equation (3.1) is

$$G_d = G_{on} \tau_d \cos \theta_z. \quad (3.11)$$

Substituting Equations (3.2), (3.3), (3.4), (3.10) and (3.11) into Equation (3.1) gives

$$\begin{aligned} G_T = & G_{on} \tau_b (\sin \delta \sin \phi \cos \beta - \sin \delta \cos \phi \sin \beta \cos \gamma + \cos \delta \cos \phi \cos \beta \cos \omega \\ & + \cos \delta \sin \phi \sin \beta \cos \gamma \cos \omega + \cos \delta \sin \beta \sin \gamma \sin \omega) \\ & + G_{on} \tau_d \cos \theta_z \left(\frac{1 + \cos \beta}{2} \right) + G_{on} \rho (\tau_b + \tau_d) \cos \theta_z \left(\frac{1 - \cos \beta}{2} \right). \end{aligned} \quad (3.12)$$

This equation still represents the three components of solar radiation impinging on the tilted panel as does Equation (3.1), but terms have been expanded to bring out the tilt dependence, β . Not emphasized in this equation is the time dependence. All quantities except, ϕ , β , and γ in equation (3.12) are a function of time and must be kept inside any time integrations that are done.

Integrating Equation (3.12) over time is done in two steps: the first step is to integrate over the hours in each of the individual days that constitute the time period of interest, and the second step is to sum over all the days in the time period of interest. For this work the time period of interest is a complete year and thus the summation will be carried out over 365 days. The reason this two-step integration process is used is solar radiation only impinges on the solar panel during the portion of the day in which the sun is above the horizon and in front of the panel. Thus, the day integration needs to be done from sunrise, t_{sr} , to sunset, t_{ss} , on the panel or sunrise, t_{sre} , to sunset, t_{sse} , on the earth depending on the term in the equation. Sunrise, t_{sr} , and sunset, t_{ss} , on the panel

can occur by the sun's position relative to the panel or the sun's position relative to the horizon of the earth. At certain times of the year sunrise and sunset on the panel are controlled by the panel; at other times sunrise and sunset are controlled by the horizon of the earth. When sunrise and sunset are controlled by the horizon of the earth $t_{sr} = t_{sre}$ and $t_{ss} = t_{sse}$ and when they are controlled by the panel itself $t_{sr} > t_{sre}$ and $t_{ss} < t_{sse}$.

Performing this time integration on Equation (3.12) gives

$$\begin{aligned}
Y_{tot} = & (\sin\phi\cos\beta - \cos\phi\sin\beta\cos\gamma) \sum_{n=1}^{365} \int_{t_{sr}}^{t_{ss}} G_{on}\tau_b\sin\delta dt \\
& + (\cos\phi\cos\beta + \sin\phi\sin\beta\cos\gamma) \sum_{n=1}^{365} \int_{t_{sr}}^{t_{ss}} G_{on}\tau_b\cos\delta\cos\omega dt \\
& + \sin\beta\sin\gamma \sum_{n=1}^{365} \int_{t_{sr}}^{t_{ss}} G_{on}\tau_b\cos\delta\sin\omega dt \\
& + (0.5 + 0.5 \cos\beta) \sum_{n=1}^{365} \int_{t_{sre}}^{t_{sse}} G_{on}\cos\theta_z\tau_d dt \\
& + (0.5 - 0.5 \rho \cos\beta) \sum_{n=1}^{365} \int_{t_{sre}}^{t_{sse}} G_{on}\cos\theta_z(\tau_b + \tau_d) dt \tag{3.13}
\end{aligned}$$

where all the quantities that are independent of time have been pulled out of the time integrals and summations. Equation (3.13) provides the total solar energy impinging on a unit area of panel over the course of one year. This equation has been grouped into five summation of integral terms, $\sum_{n=1}^{365} \int_{t_{sr}}^{t_{ss}} dt$, each one having a different integrand. The first three of these terms account for the beam radiation. This is why sunset and sunrise on the panel are used as the integration limits on the time integrals. The fourth term represents diffuse radiation from the atmosphere impinging on the solar panel. Since diffuse radiation is the same in all directions, the sun only needs to be above the horizon of the earth to have diffuse radiation incident on the front surface of the panel and the time integral limits are sunrise and sunset on the horizon of the earth. The last term in Equation (3.13) represents the ground reflected radiation. Once either the beam or diffuse radiation hits the ground they are reflected equally in all directions and are thus viewed by the panel as long as the

sun is above the horizon. Thus, the integration limits used for this term are sunrise and sunset on the horizon of the earth.

3.2. Optimum Tilt Angle Equation

The yearly solar energy incident on the solar panel per unit area, Y_{tot} , is the quantity that needs to be optimized as a function of the panel tilt angle, β . This can be done by taking the derivative of Equation (3.13) with respect to β , setting this equation equal to zero, and solving for β . In equation form this is,

$$\begin{aligned}
0 = \frac{d}{d\beta} & \left[(\sin\phi\cos\beta - \cos\phi\sin\beta\cos\gamma) \sum_{n=1}^{365} \int_{t_{sr}}^{t_{ss}} G_{on}\tau_b\sin\delta dt_d \right. \\
& + (\cos\phi\cos\beta + \sin\phi\sin\beta\cos\gamma) \sum_{n=1}^{365} \int_{t_{sr}}^{t_{ss}} G_{on}\tau_b\cos\delta\cos\omega dt_d \\
& + \sin\beta\sin\gamma \sum_{n=1}^{365} \int_{t_{sr}}^{t_{ss}} G_{on}\tau_b\cos\delta\sin\omega dt_d \\
& + (0.5 + 0.5\cos\beta) \sum_{n=1}^{365} \int_{t_{sre}}^{t_{sse}} G_{on}\cos\theta_z\tau_d dt_d \\
& \left. + (0.5\rho - 0.5\rho\cos\beta) \sum_{n=1}^{365} \int_{t_{sre}}^{t_{sse}} G_{on}\cos\theta_z(\tau_b + \tau_d) dt_d \right]. \quad (3.14)
\end{aligned}$$

This derivative must be expanded through the equation which can be done using the product rule,

$$\begin{aligned}
0 = & -\sin\phi\sin\beta \sum_{n=1}^{365} \int_{t_{sr}}^{t_{ss}} G_{on}\tau_b\sin\delta dt_d + \sin\phi\cos\beta \sum_{n=1}^{365} \frac{d}{d\beta} \int_{t_{sr}}^{t_{ss}} G_{on}\tau_b\sin\delta dt_d \\
& - \cos\phi\cos\beta\cos\gamma \sum_{n=1}^{365} \int_{t_{sr}}^{t_{ss}} G_{on}\tau_b\sin\delta dt_d - \cos\phi\sin\beta\cos\gamma \sum_{n=1}^{365} \frac{d}{d\beta} \int_{t_{sr}}^{t_{ss}} G_{on}\tau_b\sin\delta dt_d \\
& - \cos\phi\sin\beta \sum_{n=1}^{365} \int_{t_{sr}}^{t_{ss}} G_{on}\tau_b\cos\delta\cos\omega dt_d + \cos\phi\cos\beta \sum_{n=1}^{365} \frac{d}{d\beta} \int_{t_{sr}}^{t_{ss}} G_{on}\tau_b\cos\delta\cos\omega dt_d
\end{aligned}$$

$$\begin{aligned}
& + \sin\phi \cos\beta \cos\gamma \sum_{n=1}^{365} \int_{t_{sr}}^{t_{ss}} G_{on} \tau_b \cos\delta \cos\omega dt_d \\
& + \sin\phi \sin\beta \cos\gamma \sum_{n=1}^{365} \frac{d}{d\beta} \int_{t_{sr}}^{t_{ss}} G_{on} \tau_b \cos\delta \cos\omega dt_d \\
& + \cos\beta \sin\gamma \sum_{n=1}^{365} \int_{t_{sr}}^{t_{ss}} G_{on} \tau_b \cos\delta \sin\omega dt_d + \sin\beta \sin\gamma \sum_{n=1}^{365} \frac{d}{d\beta} \int_{t_{sr}}^{t_{ss}} G_{on} \tau_b \cos\delta \sin\omega dt_d \\
& - 0.5 \sin\beta \sum_{n=1}^{365} \int_{t_{sre}}^{t_{sse}} G_{on} \cos\theta_z \tau_d dt_d \\
& + 0.5 \rho \sin\beta \sum_{n=1}^{365} \int_{t_{sre}}^{t_{sse}} G_{on} \cos\theta_z (\tau_b + \tau_d) dt_d. \tag{3.15}
\end{aligned}$$

In Equation (3.15) the β derivative was moved inside the summation term because the limits of the summation are not a function of β .

To take the derivative of the integral terms, Leibnitz integral rule is used. As reported in reference [50], Leibnitz rule can be written as

$$\frac{d}{dx} \left(\int_{a(x)}^{b(x)} f(x, t) dt \right) = f(x, b(x)) \frac{db(x)}{dx} - f(x, a(x)) \frac{da(x)}{dx} + \int_{a(x)}^{b(x)} \frac{\partial}{\partial x} [f(x, t)] dt. \tag{3.16}$$

Leibnitz rule is required because the quantities t_{ss} and t_{sr} in Equation (3.15) are a function of β when the sun goes behind the panel before setting on the horizon of the earth. Since none of the quantities in the integrand of the derivative of the integral terms are a function of β , Leibnitz rule, as required here, can be simplified to

$$\frac{d}{dx} \left(\int_{a(x)}^{b(x)} f(x, t) dt \right) = f(x, b(x)) \frac{db(x)}{dx} - f(x, a(x)) \frac{da(x)}{dx}. \tag{3.17}$$

Applying Equation (3.17) to Equation (3.15) gives

$$\begin{aligned}
0 & = -\sin\phi \sin\beta \sum_{n=1}^{365} \int_{t_{sr}}^{t_{ss}} G_{on} \tau_b \sin\delta dt_d \\
& + \sin\phi \cos\beta \sum_{n=1}^{365} \left[G_{on}(t_{ss}) \tau_b(t_{ss}) \sin[\delta(t_{ss})] \frac{dt_{ss}}{d\beta} \right.
\end{aligned}$$

$$\begin{aligned}
& -G_{on}(t_{sr})\tau_b(t_{sr})\sin[\delta(t_{sr})]\frac{dt_{sr}}{d\beta}] \\
& -\cos\phi\cos\beta\cos\gamma\sum_{n=1}^{365}\int_{t_{sr}}^{t_{ss}}G_{on}\tau_b\sin\delta dt_d \\
& -\cos\phi\sin\beta\cos\gamma\sum_{n=1}^{365}\left[G_{on}(t_{ss})\tau_b(t_{ss})\sin[\delta(t_{ss})]\frac{dt_{ss}}{d\beta}\right. \\
& \quad \left.-G_{on}(t_{sr})\tau_b(t_{sr})\sin[\delta(t_{sr})]\frac{dt_{sr}}{d\beta}\right] \\
& -\cos\phi\sin\beta\sum_{n=1}^{365}\int_{t_{sr}}^{t_{ss}}G_{on}\tau_b\cos\delta\cos\omega dt_d \\
& +\cos\phi\cos\beta\sum_{n=1}^{365}\left[G_{on}(t_{ss})\tau_b(t_{ss})\cos[\delta(t_{ss})]\cos[\omega(t_{ss})]\frac{dt_{ss}}{d\beta}\right. \\
& \quad \left.-G_{on}(t_{sr})\tau_b(t_{sr})\cos[\delta(t_{sr})]\cos[\omega(t_{sr})]\frac{dt_{sr}}{d\beta}\right] \\
& +\sin\phi\cos\beta\cos\gamma\sum_{n=1}^{365}\int_{t_{sr}}^{t_{ss}}G_{on}\tau_b\cos\delta\cos\omega dt_d \\
& +\sin\phi\sin\beta\cos\gamma\sum_{n=1}^{365}\left[G_{on}(t_{ss})\tau_b(t_{ss})\cos[\delta(t_{ss})]\cos[\omega(t_{ss})]\frac{dt_{ss}}{d\beta}\right. \\
& \quad \left.-G_{on}(t_{sr})\tau_b(t_{sr})\cos[\delta(t_{sr})]\cos[\omega(t_{sr})]\frac{dt_{sr}}{d\beta}\right] \\
& +\cos\beta\sin\gamma\sum_{n=1}^{365}\int_{t_{sr}}^{t_{ss}}G_{on}\tau_b\cos\delta\sin\omega dt_d \\
& +\sin\beta\sin\gamma\sum_{n=1}^{365}\left[G_{on}(t_{ss})\tau_b(t_{ss})\cos[\delta(t_{ss})]\sin[\omega(t_{ss})]\frac{dt_{ss}}{d\beta}\right. \\
& \quad \left.-G_{on}(t_{sr})\tau_b(t_{sr})\cos[\delta(t_{sr})]\sin[\omega(t_{sr})]\frac{dt_{sr}}{d\beta}\right] \\
& -0.5\sin\beta\sum_{n=1}^{365}\int_{t_{sre}}^{t_{sse}}G_{on}\cos\theta_z\tau_d dt_d
\end{aligned}$$

$$+0.5\rho\sin\beta \sum_{n=1}^{365} \int_{t_{sr}}^{t_{ss}} G_{on}\cos\theta_z(\tau_b + \tau_d)dt_d. \quad (3.18)$$

As can be seen, this equation is quite long. It can also be noticed that the functional notation (t_{ss}) and (t_{sr}) was added to some quantities to indicate where they are evaluated. This is necessary to differentiate between quantities in the summation terms that were evaluated at the limits of the integrals.

Equation (3.18) highlights the difference between the derivation being performed here and that performed by Alhaidari [12]. Alhaidari ignored the dependence of t_{sr} and t_{ss} on β . The complication added by including this effect is great, as Equation (3.18) highlights. From physical reasoning it can be deduced that including the changing of t_{sr} and t_{ss} with β should be small. The amount of energy from the sun that reaches the surface of the earth close to sunrise and close sunset is small. Altering the tilt of the panel a little to increase the amount of time that energy is collected at sunrise and sunset should only have a small effect on the final results. Never-the-less it was an objective of this work to quantify this assumption.

Dividing Equation (3.18) by $\cos\beta$ and noting that

$$\tan\beta = \frac{\sin\beta}{\cos\beta} \quad (3.19)$$

gives

$$\begin{aligned} 0 = & -\sin\phi\tan\beta \sum_{n=1}^{365} \int_{t_{sr}}^{t_{ss}} G_{on}\tau_b\sin\delta dt_d \\ & +\sin\phi \sum_{n=1}^{365} \left[G_{on}(t_{ss})\tau_b(t_{ss})\sin[\delta(t_{ss})] \frac{dt_{ss}}{d\beta} \right. \\ & \quad \left. -G_{on}(t_{sr})\tau_b(t_{sr})\sin[\delta(t_{sr})] \frac{dt_{sr}}{d\beta} \right] \\ & -\cos\phi\cos\gamma \sum_{n=1}^{365} \int_{t_{sr}}^{t_{ss}} G_{on}\tau_b\sin\delta dt_d \\ & -\cos\phi\tan\beta\cos\gamma \sum_{n=1}^{365} \left[G_{on}(t_{ss})\tau_b(t_{ss})\sin[\delta(t_{ss})] \frac{dt_{ss}}{d\beta} \right. \end{aligned}$$

$$\begin{aligned}
& -G_{on}(t_{sr})\tau_b(t_{sr})\sin[\delta(t_{sr})]\frac{dt_{sr}}{d\beta} \\
& -\cos\phi\tan\beta\sum_{n=1}^{365}\int_{t_{sr}}^{t_{ss}}G_{on}\tau_b\cos\delta\cos\omega dt_d \\
& +\cos\phi\sum_{n=1}^{365}\left[G_{on}(t_{ss})\tau_b(t_{ss})\cos[\delta(t_{ss})]\cos[\omega(t_{ss})]\frac{dt_{ss}}{d\beta}\right. \\
& \quad \left.-G_{on}(t_{sr})\tau_b(t_{sr})\cos[\delta(t_{sr})]\cos[\omega(t_{sr})]\frac{dt_{sr}}{d\beta}\right] \\
& +\sin\phi\cos\gamma\sum_{n=1}^{365}\int_{t_{sr}}^{t_{ss}}G_{on}\tau_b\cos\delta\cos\omega dt_d \\
& +\sin\phi\tan\beta\cos\gamma\sum_{n=1}^{365}\left[G_{on}(t_{ss})\tau_b(t_{ss})\cos[\delta(t_{ss})]\cos[\omega(t_{ss})]\frac{dt_{ss}}{d\beta}\right. \\
& \quad \left.-G_{on}(t_{sr})\tau_b(t_{sr})\cos[\delta(t_{sr})]\cos[\omega(t_{sr})]\frac{dt_{sr}}{d\beta}\right] \\
& +\sin\gamma\sum_{n=1}^{365}\int_{t_{sr}}^{t_{ss}}G_{on}\tau_b\cos\delta\sin\omega dt_d \\
& +\tan\beta\sin\gamma\sum_{n=1}^{365}\left[G_{on}(t_{ss})\tau_b(t_{ss})\cos[\delta(t_{ss})]\sin[\omega(t_{ss})]\frac{dt_{ss}}{d\beta}\right. \\
& \quad \left.-G_{on}(t_{sr})\tau_b(t_{sr})\cos[\delta(t_{sr})]\sin[\omega(t_{sr})]\frac{dt_{sr}}{d\beta}\right] \\
& -0.5\tan\beta\sum_{n=1}^{365}\int_{t_{sre}}^{t_{sse}}G_{on}\cos\theta_z\tau_d dt_d \\
& +0.5\rho\tan\beta\sum_{n=1}^{365}\int_{t_{sre}}^{t_{sse}}G_{on}\cos\theta_z(\tau_b+\tau_d)dt_d. \tag{3.20}
\end{aligned}$$

Isolating $\tan\beta$ on the left-hand side of this equation gives

$$\tan\beta = \frac{A}{B}; \tag{3.21}$$

where,

$$\begin{aligned}
A = & \sin\phi \sum_{n=1}^{365} \left[G_{on}(t_{ss})\tau_b(t_{ss})\sin[\delta(t_{ss})] \frac{dt_{ss}}{d\beta} \right. \\
& \left. - G_{on}(t_{sr})\tau_b(t_{sr})\sin[\delta(t_{sr})] \frac{dt_{sr}}{d\beta} \right] \\
& - \cos\phi \cos\gamma \sum_{n=1}^{365} \int_{t_{sr}}^{t_{ss}} G_{on}\tau_b \sin\delta dt_d \\
& + \cos\phi \sum_{n=1}^{365} \left[G_{on}(t_{ss})\tau_b(t_{ss})\cos[\delta(t_{ss})]\cos[\omega(t_{ss})] \frac{dt_{ss}}{d\beta} \right. \\
& \left. - G_{on}(t_{sr})\tau_b(t_{sr})\cos[\delta(t_{sr})]\cos[\omega(t_{sr})] \frac{dt_{sr}}{d\beta} \right] \\
& + \sin\phi \cos\gamma \sum_{n=1}^{365} \int_{t_{sr}}^{t_{ss}} G_{on}\tau_b \cos\delta \cos\omega dt_d \\
& + \sin\gamma \sum_{n=1}^{365} \int_{t_{sr}}^{t_{ss}} G_{on}\tau_b \cos\delta \sin\omega dt_d
\end{aligned} \tag{3.22}$$

and

$$\begin{aligned}
B = & \sin\phi \sum_{n=1}^{365} \int_{t_{sr}}^{t_{ss}} G_{on}\tau_b \sin\delta dt_d \\
& + \cos\phi \cos\gamma \sum_{n=1}^{365} \left[G_{on}(t_{ss})\tau_b(t_{ss})\sin[\delta(t_{ss})] \frac{dt_{ss}}{d\beta} \right. \\
& \left. - G_{on}(t_{sr})\tau_b(t_{sr})\sin[\delta(t_{sr})] \frac{dt_{sr}}{d\beta} \right] \\
& + \cos\phi \sum_{n=1}^{365} \int_{t_{sr}}^{t_{ss}} G_{on}\tau_b \cos\delta \cos\omega dt_d \\
& - \sin\phi \cos\gamma \sum_{n=1}^{365} \left[G_{on}(t_{ss})\tau_b(t_{ss})\cos[\delta(t_{ss})]\cos[\omega(t_{ss})] \frac{dt_{ss}}{d\beta} \right. \\
& \left. - G_{on}(t_{sr})\tau_b(t_{sr})\cos[\delta(t_{sr})]\cos[\omega(t_{sr})] \frac{dt_{sr}}{d\beta} \right]
\end{aligned}$$

$$\begin{aligned}
& -\sin\gamma \sum_{n=1}^{365} \left[G_{on}(t_{ss})\tau_b(t_{ss})\cos[\delta(t_{ss})]\sin[\omega(t_{ss})] \frac{dt_{ss}}{d\beta} \right. \\
& \quad \left. - G_{on}(t_{sr})\tau_b(t_{sr})\cos[\delta(t_{sr})]\sin[\omega(t_{sr})] \frac{dt_{sr}}{d\beta} \right] \\
& + 0.5 \sum_{n=1}^{365} \int_{t_{sre}}^{t_{sse}} G_{on}\cos\theta_z \tau_d dt_d \\
& - 0.5\rho \sum_{n=1}^{365} \int_{t_{sre}}^{t_{sse}} G_{on}\cos\theta_z (\tau_b + \tau_d) dt_d. \tag{3.23}
\end{aligned}$$

The tilt angel can now be obtained as

$$\beta = \tan^{-1} \frac{A}{B}. \tag{3.24}$$

The β obtained from this equation is the optimum tilt angle of a fixed solar panel with beam, atmospheric diffuse, and ground reflected solar radiation components included. This is a general equation that includes all effects on the optimum tilt angle within the assumptions of Equation (3.1).

3.3. Rate of Change of Panel Sunrise and Sunset Times with Panel Tilt

This derivation is still not complete. The quantities $\frac{dt_{sr}}{d\beta}$ and $\frac{dt_{ss}}{d\beta}$ have to be obtained. The equations for $\frac{dt_{sr}}{d\beta}$ and $\frac{dt_{ss}}{d\beta}$ are exactly the same, except for the subscripts; thus, only sunrise will be looked at in this thesis. This is done by using Equations (3.4), (3.6), and the chain rule. If the chain rule is used on $\frac{dt_{sr}}{d\beta}$ it gives

$$\frac{\partial t_{sr}}{\partial \beta} = \frac{\partial t_{sr}}{\partial \omega_{sr}} \frac{\partial \omega_{sr}}{\partial \beta}. \tag{3.25}$$

The derivative $\frac{\partial t_{sr}}{\partial \omega_{sr}}$ is obtained from Equation (3.6) and the derivative $\frac{\partial \omega_{sr}}{\partial \beta}$ is obtained from Equation (3.4).

Solving Equation (3.6) for time, taking the derivative with respect to the hour angle, and solving the resultant equation at sunrise gives

$$\frac{\partial t_{sr}}{\partial \omega_{sr}} = \frac{1}{15} \frac{180}{\pi}. \tag{3.26}$$

The factor $\frac{180}{\pi}$ is added to convert the units of the derivative to per radian as opposed to per degree. This has to be done before utilizing this quantity in Equations (3.22) and (3.23).

Obtaining the derivative $\frac{\partial \omega_{sr}}{\partial \beta}$ is a little more difficult. Before taking the derivative of Equation (3.4) it needs to be recognized that the $\cos\theta$ is equal to zero at sunrise and sunset. Setting the left-hand side of Equation (3.4) to zero and taking the derivative with respect to β gives

$$\frac{\partial \omega_{sr}}{\partial \beta} = \frac{C}{D} \quad (3.27)$$

where C is

$$C = -\sin\phi\sin\beta\sin\delta_{sr} - \cos\phi\cos\beta\cos\gamma\sin\delta_{sr} - \cos\phi\sin\beta\cos\omega_{sr}\cos\delta_{sr} \\ + \sin\phi\cos\beta\cos\gamma\cos\omega_{sr}\cos\delta_{sr} + \cos\beta\sin\gamma\sin\omega_{sr}\cos\delta_{sr} \quad (3.28)$$

and D is

$$D = \cos\phi\cos\beta\sin\omega_{sr}\cos\delta_{sr} + \sin\phi\sin\beta\cos\gamma\sin\omega_{sr}\cos\delta_{sr} \\ - \sin\beta\sin\gamma\cos\omega_{sr}\cos\delta_{sr} . \quad (3.29)$$

Equations (3.24), (3.22), and (3.23) coupled with Equations (3.25) through (3.29) provide the optimum tilt angle of a solar panel at a specified location on the surface of the earth, for a specified azimuthal orientation, for a period of one year. Other time periods can easily be used by altering the limits on the summation terms in Equations (3.22) and (3.23). Equations (3.25) through (3.29) are only used when sunrise and sunset on the panel are controlled by the panel itself and these derivatives are set equal to zero when sunrise and sunset are controlled by the horizon of the earth.

Chapter 4

Atmospheric Transmissivities

Calculating beam and diffuse transmissivities for a certain time of day, for a certain day of the year, is an important factor to calculate the optimum tilt angle of a solar panel. The equations developed in Chapter 3 for the optimum tilt angle of a fixed solar panel, Equations (3.22), (3.23) and (3.24), depend on knowing the beam transmissivity, τ_b , and the diffuse transmissivity, τ_d , of the earth's atmosphere to solar radiation. Solar radiation above the earth's atmosphere, normal to the sun's rays is easily determined using Equation (3.9); however, variations in atmospheric conditions make determining how much solar energy reaches the earth's surface difficult. For this reason, atmospheric transmittance models are somewhat empirical in nature. In this work, the effects of the atmosphere, including cloud cover, are handled with beam and diffuse transmissivities. The equations used to determine both of these quantities are given in this chapter. Before discussing equations used to determine transmissivities that include cloud cover, clear sky transmissivities are discussed. Clear sky transmissivities are required because the cloud cover transmissivity equations are based on clear sky values. Before discussing any of these transmissivities, the reader is provided with definition equations for beam and diffuse transmissivities.

4.1. Definitions of Beam and Diffuse Transmissivities

The beam transmittance is the ratio of the solar radiation that reaches the surface of the earth without interacting with the earth's atmosphere, $G_{b,n}$, to the solar radiation just above the atmosphere, G_{on} ,

$$\tau_b = \frac{G_{b,n}}{G_{on}}. \quad (4.1)$$

As indicated by the subscript n , these quantities are for a surface normal to the sun's rays. Theoretically the beam transmittance can take on values between zero and one, but a value of one will never be obtained because the atmosphere always absorbs and scatters some of the solar radiation traveling through it. Replacing the ground quantity representing solar radiation normal to the sun's rays with a quantity for solar radiation on a ground horizontal surface requires division by the cosine of the zenith angle giving,

$$\tau_b = \frac{G_b}{G_{on} \cos \theta_z}. \quad (4.2)$$

The diffuse transmissivity is not a transmissivity in the strict sense of the meaning of transmissivity. Transmissivities are technically quantities that represent the fraction of the radiation that makes it through a material without interacting with the material. The diffuse transmissivity is the fraction of solar radiation scattered by the atmosphere that makes it to the earth's surface relative to the amount of solar radiation entering the top of the atmosphere. In terms of ground solar radiation on a horizontal surface this can be written as

$$\tau_d = \frac{G_d}{G_{on} \cos \theta_z}, \quad (4.3)$$

where, G_d is the amount of diffuse radiation impinging on a horizontal unit area located on the surface of the earth. While G_d can be stated as being on a horizontal surface, it can be taken to be any orientated surface. In an isotropic sky model, the diffuse radiation is assumed to be the same in all directions and thus will have the same value on any orientation of surface. The diffuse transmissivity will never reach a value as low as zero or as high as one. Because diffuse radiation is spread throughout the atmosphere from the ground level to the edge of outer space, diffuse transmissivity at the ground is much less than one. Normally diffuse transmissivities are smaller than beam transmissivities, but on very cloudy days this can reverse.

Both the beam and the diffuse transmissivities are a function of atmospheric conditions. Since whether conditions vary from day to day, hour to hour, and from location to location, this

means atmospheric transmissivities can vary from day to day, hour to hour, and location to location. In this work, representative atmospheres are used and variations from location to location are ignored. Variations from day to day and hour to hour caused by the position of the sun in the sky are included, but variations with time due to weather factors are neglected. A representative clear sky is used in this work. This representative clear atmosphere is determined by the values of the constants inserted into the transmissivity equations. Varying cloud conditions are treated as a parameter in this work.

4.2. Clear Sky Transmissivities

A clear sky is one that does not have any clouds present. The absorption and scattering of solar radiation in a clear sky are caused by the thickness and the makeup of the atmosphere. A typical clear sky is mostly made up of nitrogen and oxygen, but also includes small amounts of argon, carbon dioxide, nitrous oxides, methane, and ozone. A clear sky atmosphere will also contain varying amounts of water vapor depending on the climate.

In this work the beam transmissivity equation of Hottel [24] is used. Hottel developed a semi-empirical relationship for the beam transmissivity of a clear sky, $\tau_{b,cs}$, that accounts for the distance solar radiation travels through the atmosphere,

$$\tau_{b,cs} = a_0 + a_1 e^{\left(\frac{-k}{\cos\theta_z}\right)}. \quad (4.4)$$

Hottel [24] designed this equation so that a_0 , a_1 and k are allowed to vary as a function of ground elevation above sea level and climate type. For this work, all results are generated with representative values of $a_0 = 0.1243$, $a_1 = 0.7493$, and $k = 0.3950$. If the reader desires, equations for these three constants, for different climates and ground elevations, can be found in Duffie and Beckman [15]. A primary factor that determines the beam transmissivity is the distance the radiation travels through the atmosphere. This distance is a function of the zenith angle of the sun which is included in Equation (4.4) as $\frac{1}{\cos\theta_z}$.

A cruder clear sky beam transmissivity equation has been presented by Kasten and Czeplak [17],

$$\tau_{b,cs} = 0.47 - \frac{0.016}{\cos\theta_z}. \quad (4.5)$$

It is immediately obvious that this equation is not exactly the same as the equation put forth by Hottel [24] shown in Equation (4.4). First, this equation has the constants a_0 and a_1 filled with numerical values. This does not make Equation (4.5) significantly different than Equation (4.4), because the values of 0.47 and 0.016 can easily be changed. Kasten and Czeplak [17] have these two particular values in this equation because they were specifically looking at Hamburg, Germany in their work. The more important difference is that Kasten and Czeplak do not have the $\frac{1}{\cos\theta_z}$ quantity inside an exponential function. Transmissivities of radiation traversing an absorbing emitting medium tend to follow Beer's Law [51] which shows a decreasing exponential dependence of transmittance on increasing distance travelled through the absorbing and scattering medium. Thus, it is concluded that Hottel's [24] expression for beam transmissivity is more physically based than that of Kasten and Czeplak [17]. Kasten and Czeplak's equation does show a decreasing beam transmissivity with increasing distance, but it is not an exponentially decreasing beam transmittance. Keeping the length term, $\frac{1}{\cos\theta_z}$, outside of an exponential function produces unrealistic results in certain situations as is shown in Figure 4.1.

Figure 4.1 shows the clear sky beam transmissivities from Hottel's model [24] (Equation 4.4) and those from Kasten and Czeplak's model [17] (Equation 4.5) at a 40° latitude, for June 21, as a function of time of day. The beam transmissivities are set to zero at night and only take on nonzero values during the time when the sun is above the horizon. Large differences can be seen in the predicted transmissivities of Hottel and Kasten and Czeplak. In addition to the magnitude differences, there are shape differences. Hottel's results are more rounded and Kasten and Czeplak's results are flatter. Lastly, Kasten and Czeplak's model produces negative beam transmissivities, while Hottel's model does not. These negative values are caused by the second term on the right-hand side of Equation (4.5). When the zenith angle becomes close to 90° the second term becomes very large. From Equation (4.4) it can be seen that Hottel's model will never produce negative beam transmittance values when positive coefficients are inserted. Negative transmissivities should not be predicted, and this behaviour shows the more empirical nature of Kasten and Czeplak's model compared to Hottel's model.

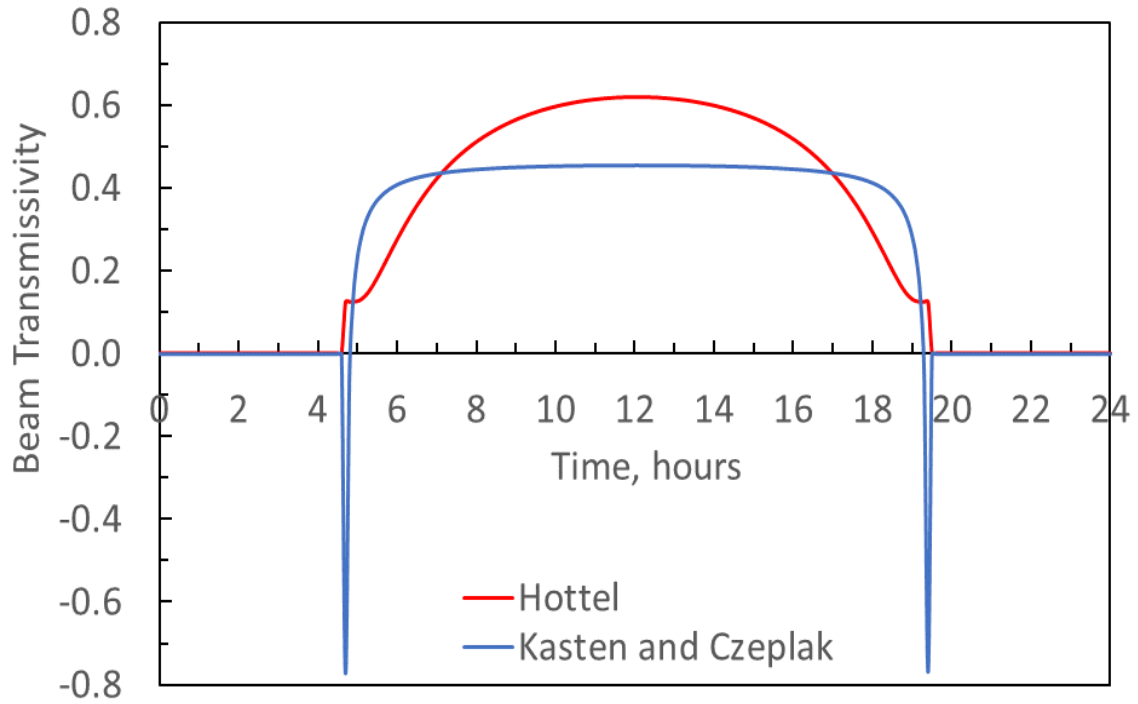


Figure 4.1: Clear sky beam transmissivities from the model of Hottel [24] and from the model of Kasten and Czeplak [17] for June 21, at a latitude of 40°.

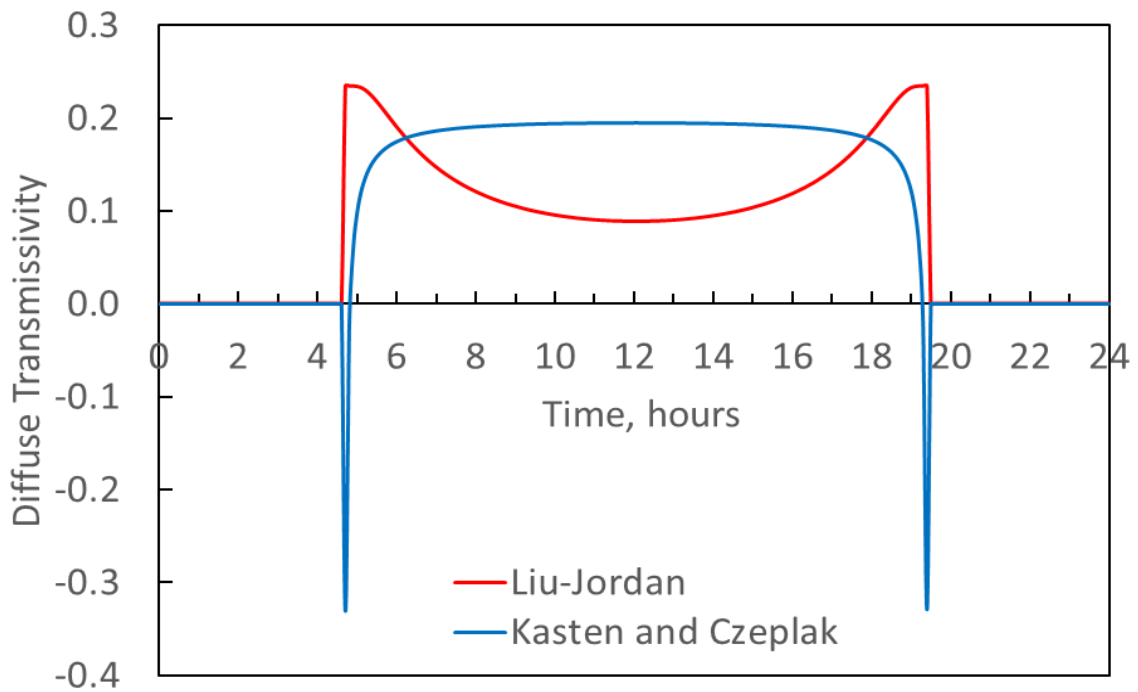


Figure 4.2: Clear sky diffuse transmissivities from the model of Liu and Jordan [18] and from the model of Kasten and Czeplak [17] for June 21, at a latitude of 40°.

The clear sky diffuse transmissivity used in this work for clear sky conditions, $\tau_{d,cs}$, was developed by Lui and Jordan [18]. Lui and Jordan developed an equation to calculate the diffuse transmissivity that is dependent on the beam transmissivity,

$$\tau_{d,cs} = 0.271 - 0.294\tau_{b,cs}. \quad (4.6)$$

At first glance this looks like a linear equation, that is not dependent on the distance the solar radiation travels through the atmosphere. This is not the case, because $\tau_{b,cs}$ is an exponential function of the distance the radiation travels through the atmosphere. Thus, the diffuse transmittance has a similar equation form to the beam transmittance, except for the negative sign. It may seem that this negative sign makes negative diffuse transmissivities possible, but it does not. The largest beam transmissivity produced by Equation (4.4) with the constants used for this work is 0.874, which means Equation (4.6) always produces positive diffuse transmissivities.

A clear sky diffuse beam transmissivity model implied by Kasten and Czeplak [17] is

$$\tau_{d,cs} = 0.43\tau_{b,cs}. \quad (4.7)$$

Quite obviously this equation causes the clear sky diffuse transmissivity to follow the trend of the clear sky beam transmissivity. This is in contrast to the clear sky diffuse transmissivity provided by Liu and Jordan [18]. Liu and Jordan show the diffuse transmissivity increasing as the beam transmissivity decreases. Liu and Jordan's diffuse transmissivity trends make more sense than those of Kasten and Czeplak because diffuse radiation comes at the expense of the beam radiation. More scattering in the atmosphere leads to less beam radiation and more diffuse radiation. Of course, this line of reasoning breaks down for heavy cloud cover because much of the scattering occurs at higher elevations and does not make it to the ground to become the diffuse solar radiation, G_d , given in Equation (4.3).

Figure 4.2 shows the clear sky diffuse transmissivities from Liu-Jordan model [18] (Equation 4.4) and Kasten and Czeplak's [17] model (Equation 4.7) at a 40° latitude, for June 21, as a function of time of day. These diffuse transmissivities were determined from the beam transmissivities shown in Figure 4.1. Kasten and Czeplak's results do not show the same trends as Liu and Jordan's [18] results. Liu and Jordan's results show the diffuse transmissivity being larger towards sunrise and sunset as it should. Also, Kasten and Czeplak's model produces negative values, while Hottel's model and Liu and Jordan's model do not. Just like beam transmissivities, diffuse transmissivities should never take on negative values. Because Hottel's model and Liu and

Jordan's model are much more physically realistic than Kasten and Czeplak's model, it is the one used in this work to determine beam and diffuse transmittances.

4.3. Cloudy Transmissivities

The reason for using Kasten and Czeplak's [17] work on atmospheric transmissivities is that they provide a simple means of handling cloud cover. Other cloud models exist such as the meteorological radiation model [52] and the Page radiation model [53], but they are complex and require large amounts of tabulated data. In Kasten and Czeplak's [17] model, the amount of cloud cover is defined by a quantity N which is given in oktas. An okta is the number of eighths present and varies from 0 to 8 where 0 is a clear sky and 8 is a completely overcast sky. Thus, changing the N from 0 to 8 varies the cloud cover, making parameter surveys of the effect of cloud cover easy to do. In this work, the Kasten-Czeplak model is used to obtain cloud cover beam, $\tau_{b,cc}$, and diffuse, $\tau_{d,cc}$, transmissivities from clear sky transmissivities.

The equations taken from Kasten-Czeplak [17] to determine the beam and diffuse transmissivities are written in terms of global solar radiation quantities as

$$\frac{G}{G_{cs}} = 1 - 0.75 \left(\frac{N}{8} \right)^{3.4} \quad (4.8)$$

and

$$\frac{G_d}{G} = C + D \left(\frac{N}{8} \right)^2, \quad (4.9)$$

where Kasten and Czeplak have set $C = 0.3$ and $D = 0.7$. In these equations G and G_d are the total and diffuse radiation falling on a horizontal surface as a function of the amount of cloud cover. The quantities G and G_d are the same as defined in Chapter 3. The quantity G_{cs} is physically the same as G , but is evaluated for clear sky conditions. Equation (4.8) shows that G takes on the value of G_{cs} when there are no clouds in the sky. Equations (4.8) and (4.9) need to be written in terms of transmissivities to be inserted into Equations (3.22) and (3.23). This can be done using the definitions of the beam and diffuse transmissivities given in Equations (4.2) and (4.3).

As shown in Equations (3.2) both G and G_{cs} can be written as the sum of the beam and diffuse components. Doing this for each of these quantities and dividing every term by $G_{on} \cos \theta_z$ gives

$$\frac{G}{G_{on} \cos \theta_z} = \frac{G_b}{G_{on} \cos \theta_z} + \frac{G_d}{G_{on} \cos \theta_z} \quad (4.10)$$

and

$$\frac{G_{cs}}{G_{on} \cos \theta_z} = \frac{G_{b,cs}}{G_{on} \cos \theta_z} + \frac{G_{d,cs}}{G_{on} \cos \theta_z}. \quad (4.11)$$

From Equations (4.2) and (4.3) it can be seen that the first term on the right-hand side of both of these equations is the beam transmissivity and the second term on the right-hand side is the diffuse transmissivity giving,

$$\frac{G}{G_{on} \cos \theta_z} = \tau_b + \tau_d \quad (4.12)$$

and

$$\frac{G_{cs}}{G_{on} \cos \theta_z} = \tau_{b,cs} + \tau_{d,cs}. \quad (4.13)$$

These equations can now be solved for G and G_{cs} giving,

$$G = (\tau_b + \tau_d) G_{on} \cos \theta_z \quad (4.14)$$

and

$$G_{cs} = (\tau_{b,cs} + \tau_{d,cs}) G_{on} \cos \theta_z. \quad (4.15)$$

Substituting Equations (4.14) and (4.15) into Equation (4.8) provides a relationship for the cloud cover transmissivities as a function of the clear sky transmissivities,

$$\tau_b + \tau_d = (\tau_{b,cs} + \tau_{d,cs}) \left[1 - 0.75 \left(\frac{N}{8} \right)^{3.4} \right]. \quad (4.16)$$

Substituting Equation (4.14) into equation (4.9) and using the definition of the diffuse transmissivity, Equation (4.3), gives

$$\tau_d = (\tau_b + \tau_d) \left[C + D \left(\frac{N}{8} \right)^2 \right]. \quad (4.17)$$

Once clear sky beam and diffuse transmissivities have been obtained from Equations (4.4) and (4.6), the quantity $\tau_b + \tau_d$ can be obtained from Equation (4.16) as a function of the desired cloud cover in oktas. Using this result the quantity τ_d can be obtained from Equation (4.17). Lastly τ_b can be obtained from

$$\tau_b = (\tau_b + \tau_d) - \tau_d. \quad (4.18)$$

These equations provide the cloud cover transmissivities based on the unaltered Kasten-Czeplak [17] cloud cover-model.

4.4. Adjustments to Kasten and Czeplak Model

Because Kasten-Czeplak's cloud model [17], Equations (4.16) and (4.17), was designed to be used with Kasten-Czeplak's clear sky model, Equations (4.5) and (4.7), a problem results when another clear sky model is coupled to Kasten-Czeplak's cloud model. These problems can be seen by studying Equation (4.17). Equation (4.17) has two constants C and D where Kasten-Czeplak set $C = 0.3$ and $D = 07$.

When $N = 0$ Equation (4.17) becomes

$$\frac{\tau_{d,cs}}{\tau_{b,cs} + \tau_{d,cs}} = C. \quad (4.19)$$

Finding this ratio from the Hottel [24] and Liu and Jordan [18] models gives,

$$\begin{aligned} \frac{\tau_{d,cs}}{\tau_{b,cs} + \tau_{d,cs}} &= \frac{0.271 - 0.294\tau_{b,cs}}{0.1243 + 0.7493e^{\left(\frac{-0.3950}{\cos\theta_z}\right)} + 0.271 - 0.294\tau_{b,cs}} \\ &= \frac{0.271 - 0.294\tau_{b,cs}}{0.3953 + 0.7493e^{\left(\frac{-0.3950}{\cos\theta_z}\right)} - 0.294\tau_{b,cs}}. \end{aligned} \quad (4.20)$$

where the values for a_0 , a_1 and k have been substituted into Equation (4.4). Obviously, Equation (4.20) will not provide a value of 0.3 for $\frac{\tau_{d,cs}}{\tau_{b,cs} + \tau_{d,cs}}$ for all sun zenith angles. To keep the cloud model consistent with the clear sky model for a value of $N = 0$, a change must be made to the constant C . Equation (4.19) provides this value of C and this is the value of C used in this work. Instead of being a nonchanging number, C now varies with the distance the solar radiation travels through the atmosphere.

Once the value of C is updated to the value given by Equation (4.19), the value of D does not have the correct value for the limiting case of complete cloud cover. This problem can be seen by evaluating equation (4.17) at $N = 8$ giving,

$$\tau_d = (\tau_b + \tau_d)[C + D]. \quad (4.21)$$

For full cloud cover the beam transmissivity should go to zero; thus, Equation (4.21) becomes,

$$\tau_d = \tau_d[C + D]. \quad (4.22)$$

This equation shows that D should take on the value,

$$D = 1 - C = 1 - \frac{\tau_{d,cs}}{\tau_{b,cs} + \tau_{d,cs}}. \quad (4.23)$$

Using these new coefficients in Equation (4.17) gives,

$$\tau_d = (\tau_b + \tau_d) \left[\frac{\tau_{d,cs}}{\tau_{b,cs} + \tau_{d,cs}} + \left(1 - \frac{\tau_{d,cs}}{\tau_{b,cs} + \tau_{d,cs}} \right) \left(\frac{N}{8} \right)^2 \right]. \quad (4.24)$$

Equation (4.16) can be used to eliminate $(\tau_b + \tau_d)$ from this equation to get an equation that can be directly solved for the cloudy diffuse transmissivity once the clear sky transmissivities are known,

$$\tau_d = \left[1 - 0.75 \left(\frac{N}{8} \right)^{3.4} \right] \left[\tau_{d,cs} + \tau_{b,cs} \left(\frac{N}{8} \right)^2 \right]. \quad (4.25)$$

The sum of the cloudy beam and diffuse transmissivities can be obtained from Equation (4.16) and then the cloudy beam transmissivity can be obtained from Equation (4.18).

The complete transmissivity model used in this work is the combination of the Hottel [24], Liu and Jordan [18], and the Kasten-Czeplak [17] models. This includes Equations (4.4), (4.6), (4.25), (4.16), and (4.18). Using these equations, the clear sky beam transmissivity, the clear sky diffuse transmissivity, the cloudy sky beam transmissivity, and the cloudy sky diffuse transmissivity were calculated for June 21 and December 21. The June 21 results are shown in Figure 4.3 and the December 21 results are presented in Figure 4.4. Both of these cases are for a latitude of 40° . These figures show that the clear sky beam transmissivities are larger than the cloudy sky beam transmissivities and the cloudy sky diffuse transmissivities are larger than the clear sky diffuse transmissivities. For both clear and cloudy skies, the beam transmissivities are larger than the diffuse transmissivities. It can also be seen that clouds increase the amount of diffuse radiation over that of a clear sky, but reduce the beam radiation. All December 21 results are less than the corresponding June 21 results. This is due to the sun being lower in the sky in the winter as compared to the summer. The other obvious difference between the June 21 results and the December 21 results is the length of the time the sun is shining. The time the sun is above the horizon for June 21 is noticeably longer than that for December 21.

The transmissivity models developed in this chapter can now be used in the optimum tilt model developed in Chapter 3. Beam and diffuse transmissivities need to be calculated before Equations (3.22) through (3.24) can be solved for an optimum tilt angle.

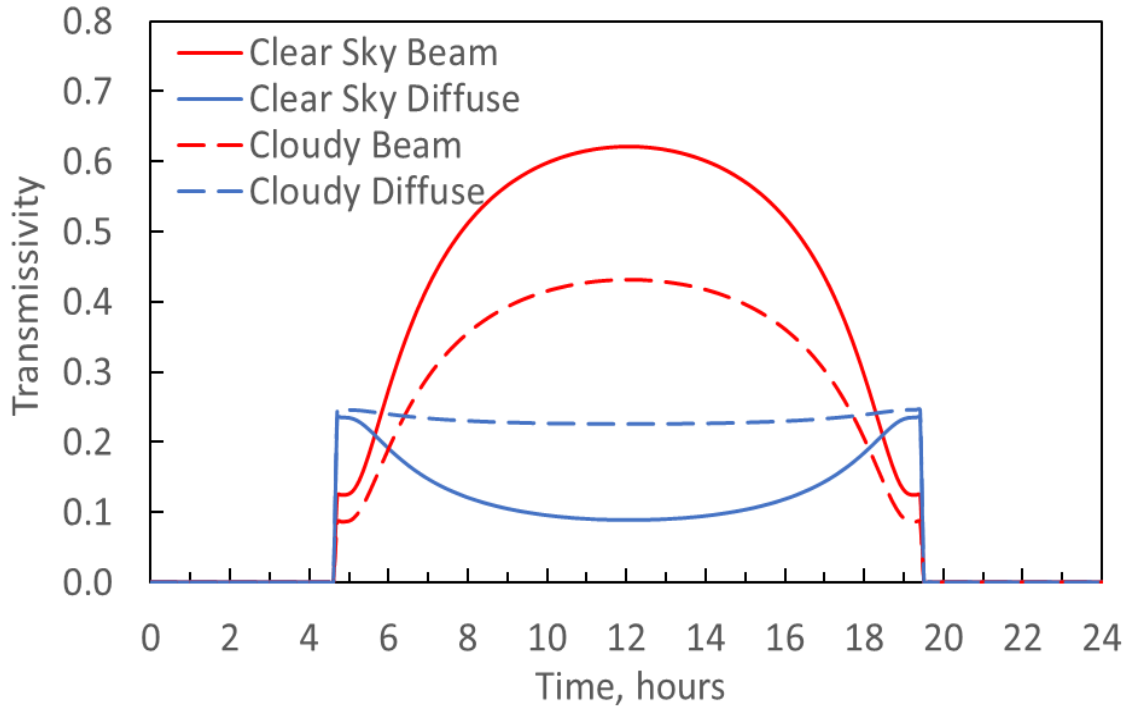


Figure 4.3: Transmissivities determined from the model developed in this work for June 21, at a latitude of 40° where the cloudy results are at 4 oktas.

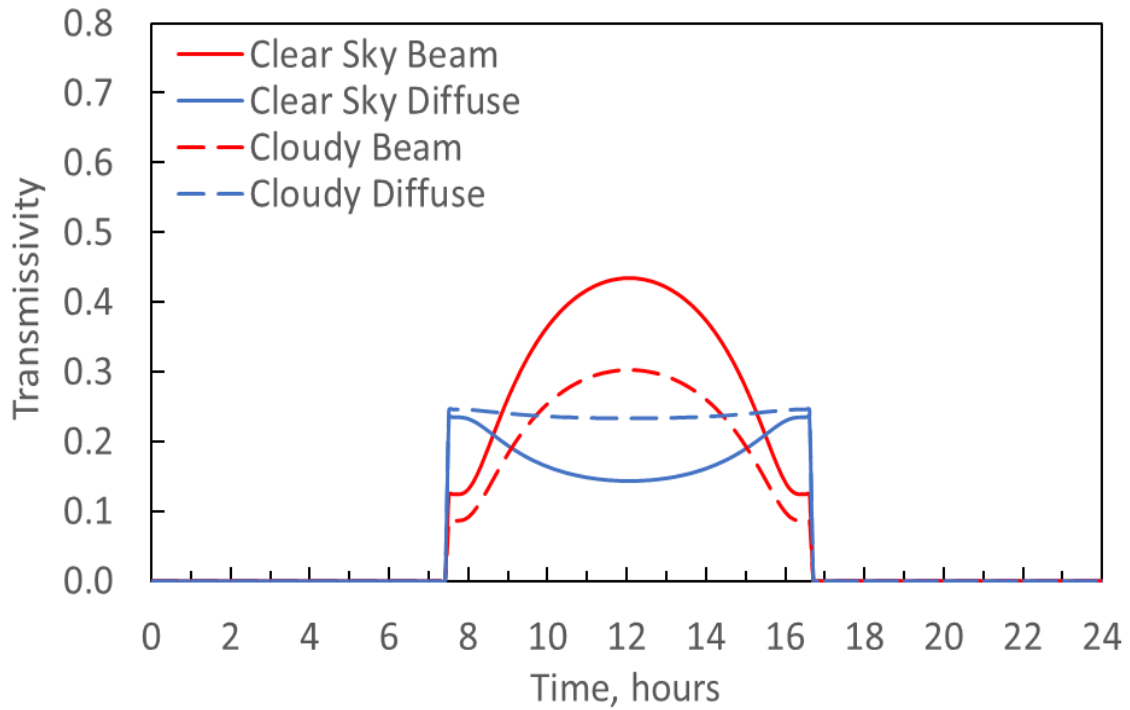


Figure 4.4: Transmissivities determined from the model developed in this work for December 21, at a latitude of 40° where the cloudy results are at 4 oktas.

Chapter 5

Results

This chapter deals with the results calculated using the equation of optimum tilt derived in Chapter 3 and the transmissivity model developed in Chapter 4. Results are displayed in four sections: the first section displays the effect of including the derivative of the integral terms, the second section displays results for uniform cloud cover conditions throughout the year, the third section displays the effects of semi-annual cloud changes, and the fourth section displays the effects of semi-daily cloud changes. The results presented in all of these sections are the tilt angle of the panel that intercepts the maximum amount of solar energy and the maximum amount of solar energy collected over a year time period per unit area of collection surface. The latitude of the location of the solar panel is treated as the independent variable and the azimuthal angle of the solar panel and the amount of cloud cover are treated as parameters.

For uniform cloud cover conditions, results for Okta numbers, N , of 0, 2, 4, 6 and 8 are presented, where an Okta number of 0 represents a completely clear sky and 8 represents a completely overcast sky. An Okta number of 4 means the cloud conditions are halfway between clear and completely overcast. To cover these five okta numbers, five plots of optimum tilts and five plots of optimum energies are presented. These results provide the reader a clear understanding of the effects of clouds on optimum tilt and maximum energy interception. They will also show the reader how these quantities vary with latitude and azimuthal orientation. Results are presented for the entire world and all eastward azimuthal orientations. Westward azimuthal orientations are not presented because their differences from the eastward orientations are unnoticeable on plots.

This occurs because the sun's path through the sky is symmetric around solar noon if the declination angle is held constant throughout the day. This work uses a varying declination angle throughout the day, but the variance is small over the course of one day.

In the case of semi-annual changing cloud cover, essentially a two-season year is considered, namely summer and winter. The months from April through September are given an Okta number of 0 and the months from October through March are given an Okta number of 6. This provides a cloudy winter and clear summer in the Northern Hemisphere and a cloudy summer and clear winter in the Southern hemisphere. The same values of Okta number are not used for the same seasons in the different hemispheres to show the reader that the season in which the cloud cover occurs affects the optimum tilt angle significantly.

In the case of semi-daily varying cloud cover, the day is divided into two parts: morning, which comprises sunrise to solar noon, and afternoon, which comprises solar noon to sunset. For the Northern Hemisphere, the Okta number is taken to be 0 in the morning and 6 in the afternoon. For the Southern Hemisphere, the Okta numbers are reversed having 6 in the morning and 0 in the afternoon. The values of Okta number are flipped in each hemisphere to show the contrast of results for different amounts of cloud cover for different parts of the day.

In each of the graphs presented in this chapter, the horizontal axis represents the latitude under consideration and the vertical axis represents the optimum tilt or maximum energy depending on the graph. Latitudes are taken with an increment of 1° . Each graph displays results for seven azimuthal angles, which are $-180^\circ/-0^\circ$, $-165^\circ/-15^\circ$, $-150^\circ/-30^\circ$, $-135^\circ/-45^\circ$, $-120^\circ/-60^\circ$, $-105^\circ/-75^\circ$ and $-90^\circ/-90^\circ$. The obtuse azimuthal angles represent those in the Southern Hemisphere and the acute azimuthal angles represents those in the Northern Hemisphere. These obtuse and acute azimuthal angles are counterparts to each other, as the panel should be facing southward in the Northern Hemisphere and northward in the Southern Hemisphere. The negative sign on the azimuthal angles provides easterly azimuthal angle orientations. This means that the panel is facing the morning sun. Each azimuthal angle on each plot is defined by a particular color: $-180^\circ/-0^\circ$ is purple, $-165^\circ/-15^\circ$ is brown, $-150^\circ/-30^\circ$ is yellow, $-135^\circ/-45^\circ$ is green, $-120^\circ/-60^\circ$ is red, $-105^\circ/-75^\circ$ is blue and $-90^\circ/-90^\circ$ is black. This should help the reader make comparisons between different graphs.

5.1. Effect of Derivative of the Integral Terms

In the equation developed by Alhaidari [12] (Equations 2.3 – 2.5) to calculate the optimum tilt of a solar panel, terms were ignored to make the calculations simpler. These terms account for varying energy collection at sunrise and sunset as the panel tilt is changed. The terms that account for this effect are being called the derivative of the integral terms in this thesis. In this thesis, the optimum tilt equations were rederived including the derivative of the integral terms and are given in Equations (3.22) through (3.25). As can be seen, a great deal of complication is added when the variation in energy collection with panel tilt at sunrise and sunset is included. Remember, Equations (3.25) through (3.29) are required to solve Equations (3.22) through (3.25) and Equation (3.28) and (3.29) need to be solved iteratively with the equations for sunrise and sunset times.

Table 5.1 and Table 5.2 show some results from these two versions of the optimum tilt equations. The optimum tilts with the derivative of the integral terms and those without the derivative of integral terms, as well as the maximum energy fluxes associated with these optimum tilts, are shown for only one azimuthal orientation and a few latitudes. Only a few latitudes in the Southern and Northern Hemispheres are shown for azimuthal orientations of $-90^{\circ}/90^{\circ}$ because they are the only ones that have any meaningful differences in the results between the two models. All azimuthal angles and all latitudes were calculated and compared, but only results that show a deviation greater than 5×10^{-4} degrees are given in the tables. The only changes seen were at azimuthal angles of $-90^{\circ}/90^{\circ}$ in the region of the Arctic and Antarctic circles. Table 5.1 shows these results for clear sky conditions and Table 5.2 shows these results for an Okta number of 4.

These tables, and the fact that any latitudes and azimuthal angles not shown in these tables have differences less than 5×10^{-4} degrees, indicate that the derivative of the integral terms are insignificant. While there are some large differences in the optimum tilt angles shown in Table 5.1 and Table 5.2, there are little differences in the solar energy incident on the surfaces. The largest difference in maximum incident energy is 1.8% between the two methods. These large differences in optimum tilt angles do not translate to large differences in the maximum energy collected. The reason for the small differences in energy collected can be understood by looking ahead to Figure 5.1 and Figure 5.5. For azimuthal angles of $-90^{\circ}/90^{\circ}$, the optimum tilt angles abruptly change from values of zero to some higher value for latitudes close to the Arctic and Antarctic Circles. When the derivative of the integral terms are included in the simulations, this change point moves to larger magnitudes of latitude. The small shifts of this change point to larger latitude magnitudes

have little effect on the maximum incident energy. The maximum energy remains a smooth function as can be seen in Figure 5.2 and Figure 5.6.

The effect of cloud cover on the importance of the derivative of the integral terms can be seen by looking at Table 5.2 results which have an Okta number of 4. Similar differences to those in Table 5.1 can be seen. Once again only the $-90^{\circ}/90^{\circ}$ azimuthal angle orientations show differences greater than 5×10^{-4} degrees. Similar behavior was seen for other values of the Okta number. For completely cloudy skies, $N = 8$, there are no differences. Therefore, it can be concluded that the optimum tilt angle equation developed in Chapter 3 that includes the derivative of the integral terms, does not have any significant effect on the calculated maximum energy that can be collected by fixed solar panels. There are noticeable differences in the optimum tilt angle for $-90^{\circ}/90^{\circ}$ azimuthal angle orientations at latitudes around the Arctic and Antarctic circles, but these differences do not translate into noticeable energy collection differences over the course of a year.

Table 5.1: Comparisons of optimum tilt and maximum incident energy results without the derivative of the integral terms and with the derivative of the integral terms for $-90/90$ azimuthal angles and $N = 0$.

Latitude (degrees)	Optimum Tilt Angle without the Derivative of the Integral Terms (degrees)	Optimum Tilt Angle with the Derivative of the Integral Terms (degrees)	Optimum Energy without the Derivative of the Integral Terms (kW-h/m ²)	Optimum Energy with the Derivative of the Integral Terms, (kW-h/m ²)
Southern Latitudes				
-76	45.11	45.11	891.2	891.2
-75	43.28	0	900.1	901.1
-74	41.11	0	910.1	916
-73	38.39	0	921.5	931.9
-72	34.41	0	934.3	948.7
-71	0	0	966.5	966.5
Northern Latitudes				
71	0	0	924.1	924.1
72	35.18	0	893.9	906.4
73	38.83	0	881.2	889.7
74	41.45	0	869.9	874.1
75	43.56	43.56	859.9	859.9

Table 5.2: Comparisons of optimum tilt and maximum incident energy results without the derivative of the integral terms and with the derivative of the integral terms for -90/90 azimuthal angles and N = 4.

Latitude (degrees)	Optimum Tilt Angle without the Derivative of the Integral Terms (degrees)	Optimum Tilt Angle with the Derivative of the Integral Terms (degrees)	Optimum Energy without the Derivative of the Integral Terms (kW-h/m ²)	Optimum Energy with the Derivative of the Integral Terms, (kW-h/m ²)
Southern Latitudes				
-84	43.84	43.84	754.5	754.5
-83	43.07	0	758.5	759.5
-82	42.16	0	763.1	766.1
-81	41.07	0	768.6	773.5
-80	39.79	0	774.8	781.8
-79	38.24	0	781.9	791.1
-78	36.33	0	789.8	801.2
-77	33.79	0	798.9	812.3
-76	28.74	0	809.2	824.2
-75	0	0	837.2	837.2
Southern Latitudes				
75	0	0	798.3	798.3
76	30.30	0	771.9	785.5
77	34.27	0	761.8	773.7
78	36.68	0	752.9	762.8
79	38.53	0	745.0	752.7
80	40.05	0	738.0	743.6
81	41.32	0	731.8	735.4
82	42.38	0	726.5	728.0
83	43.29	43.29	721.8	721.8

Even though the differences between the results from the model including the derivative of the integral terms and the model without the derivative of the integral terms is insignificant, all the remaining results presented in this thesis include the derivative of the integral terms.

5.2. Uniform Cloud Cover throughout the Year

Results for varying amounts of uniform cloud cover are shown in Figure 5.1 through Figure 5.10, both the optimum tilt angles and the energy incident on a solar panel at these optimum tilt angles. These energies are the maximum possible incident energy at the specified latitude and

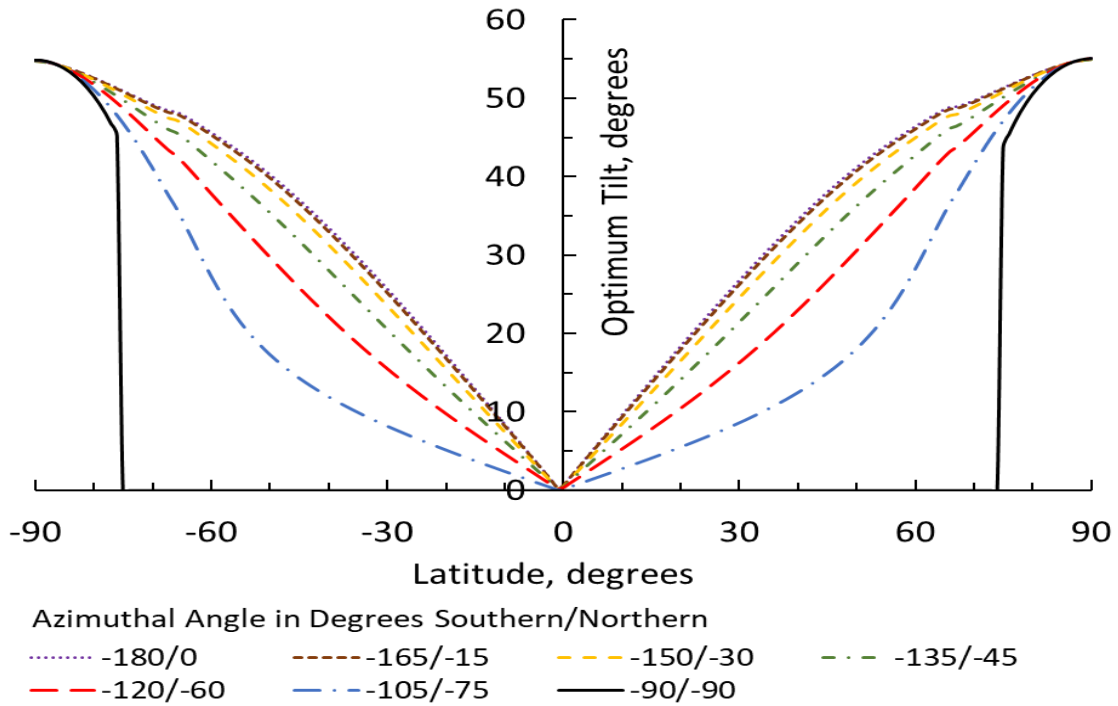


Figure 5.1: Yearly optimum tilt angles for a uniform value of $N = 0$ throughout the year.

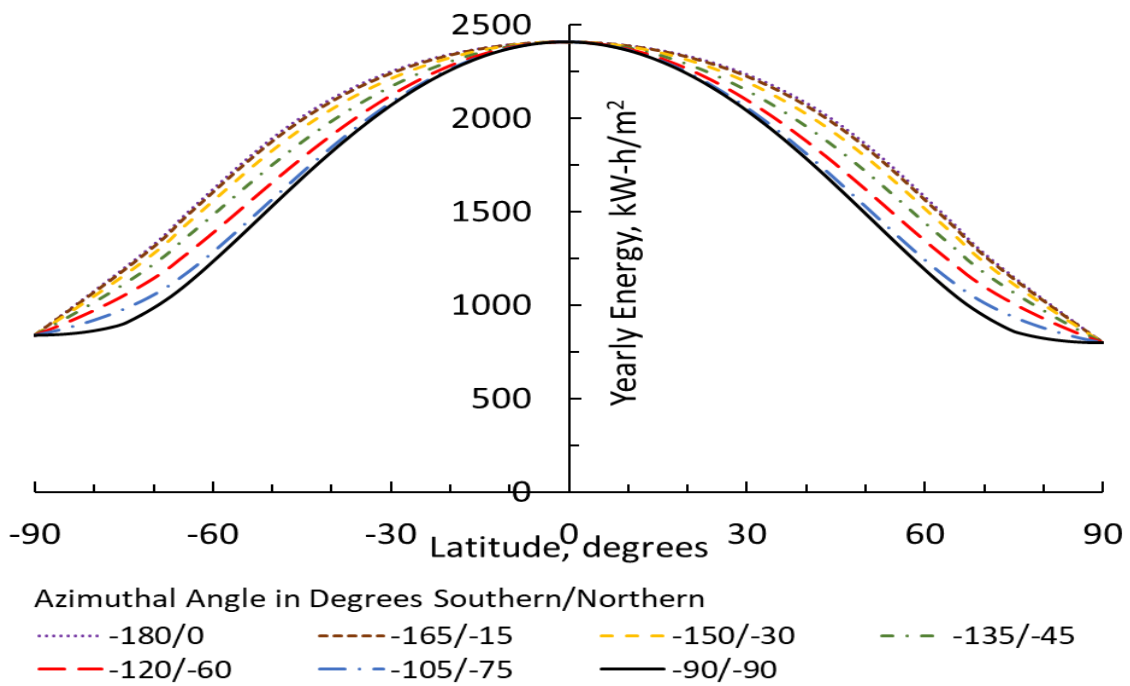


Figure 5.2: Yearly maximum intercepted energy for a uniform value of $N = 0$ throughout the year.

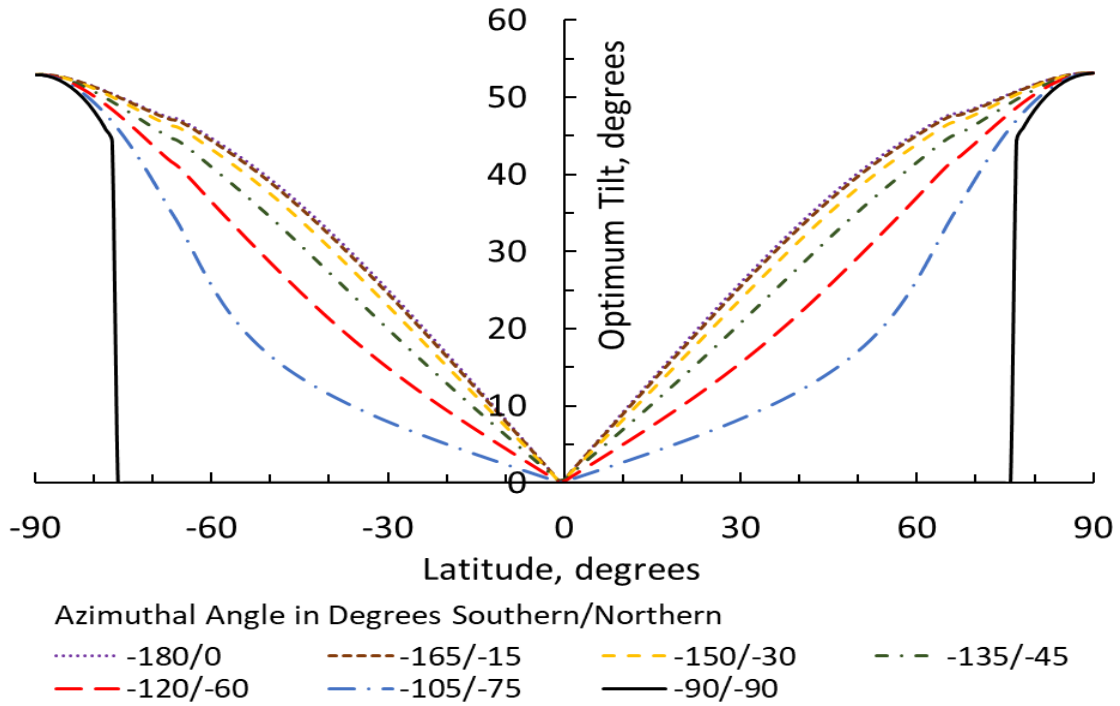


Figure 5.3: Yearly optimum tilt angles for a uniform value of $N = 2$ throughout the year.

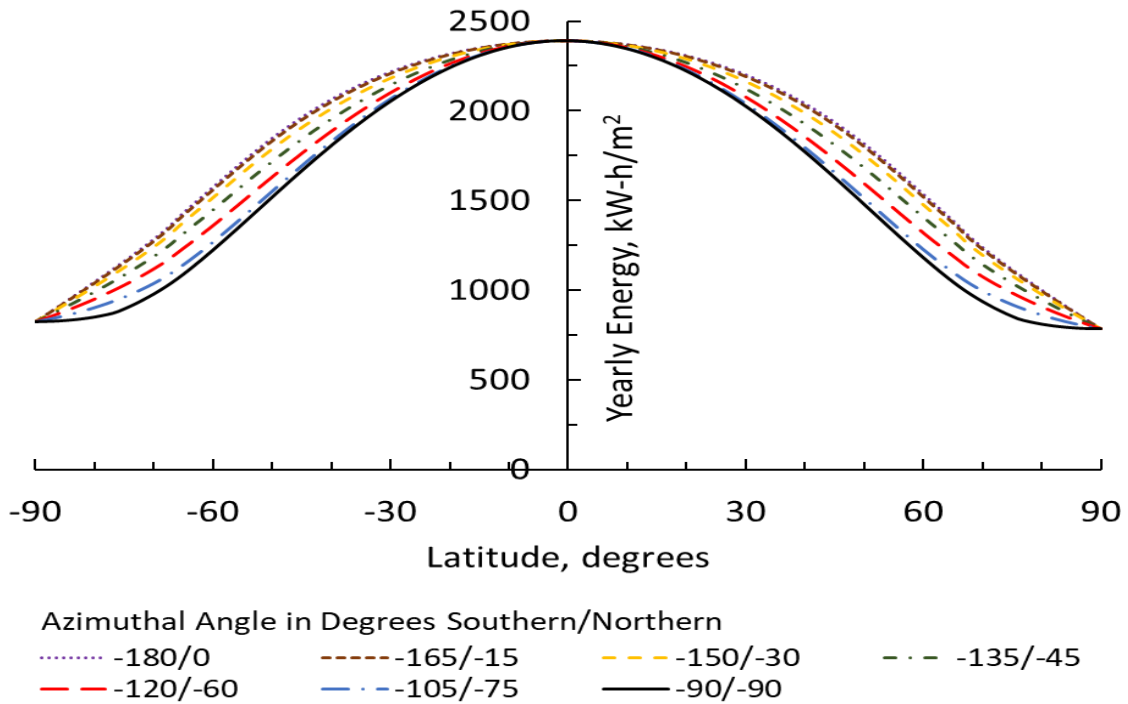


Figure 5.4: Yearly maximum intercepted energy for a uniform value of $N = 2$ throughout the year.

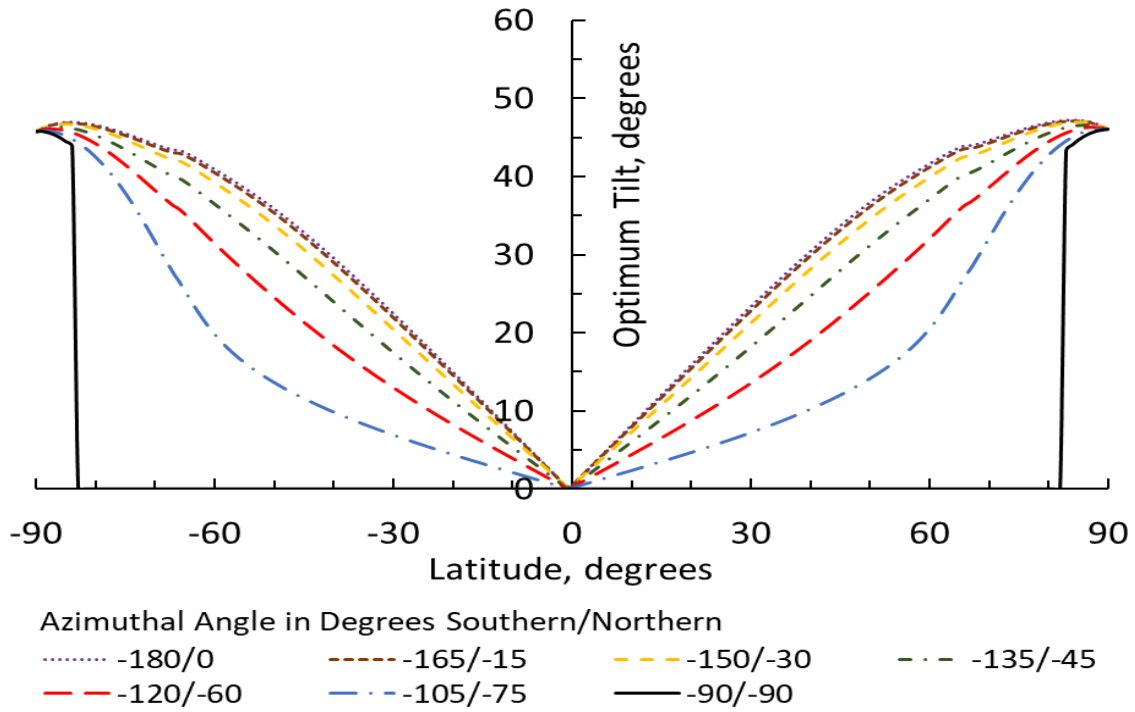


Figure 5.5: Yearly optimum tilt angles for a uniform value of $N = 4$ throughout the year.

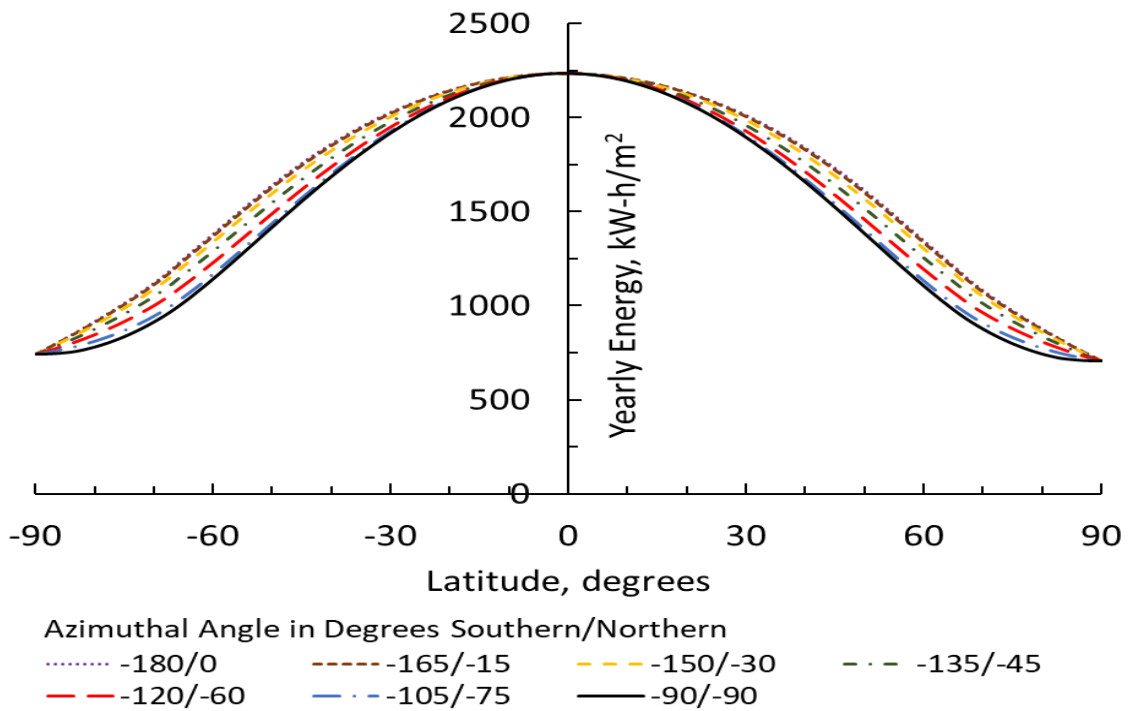


Figure 5.6: Yearly maximum intercepted energy for a uniform value of $N = 4$ throughout the year.

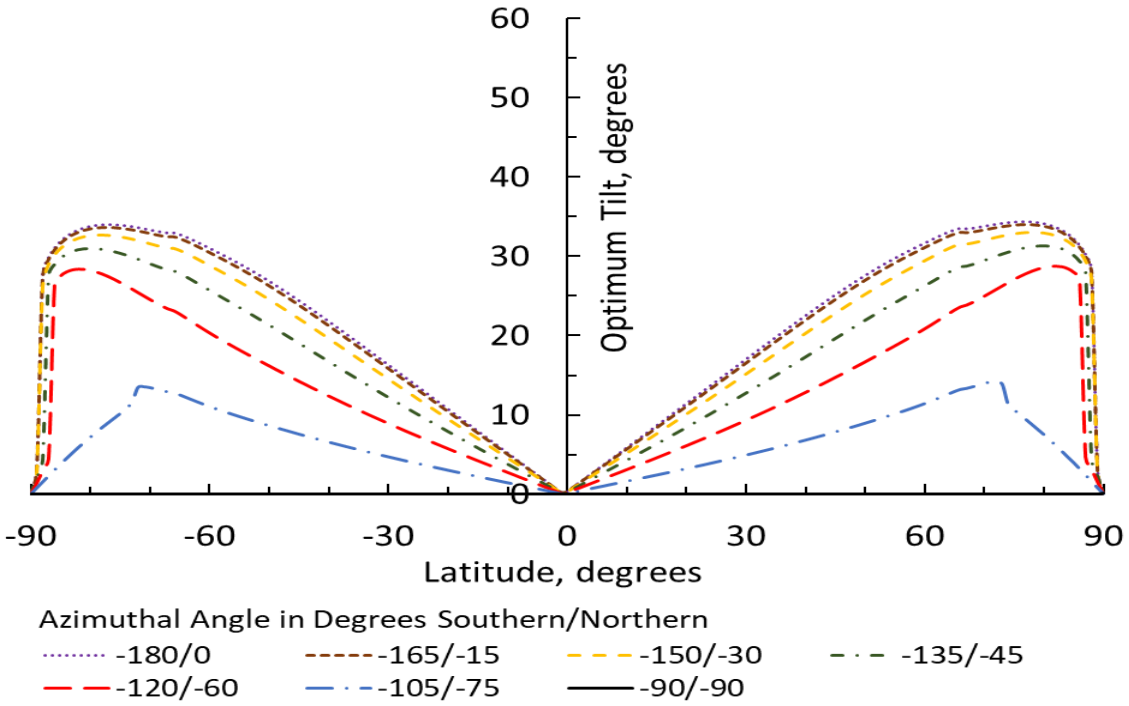


Figure 5.7: Yearly optimum tilt angles for a uniform value of $N = 6$ throughout the year.

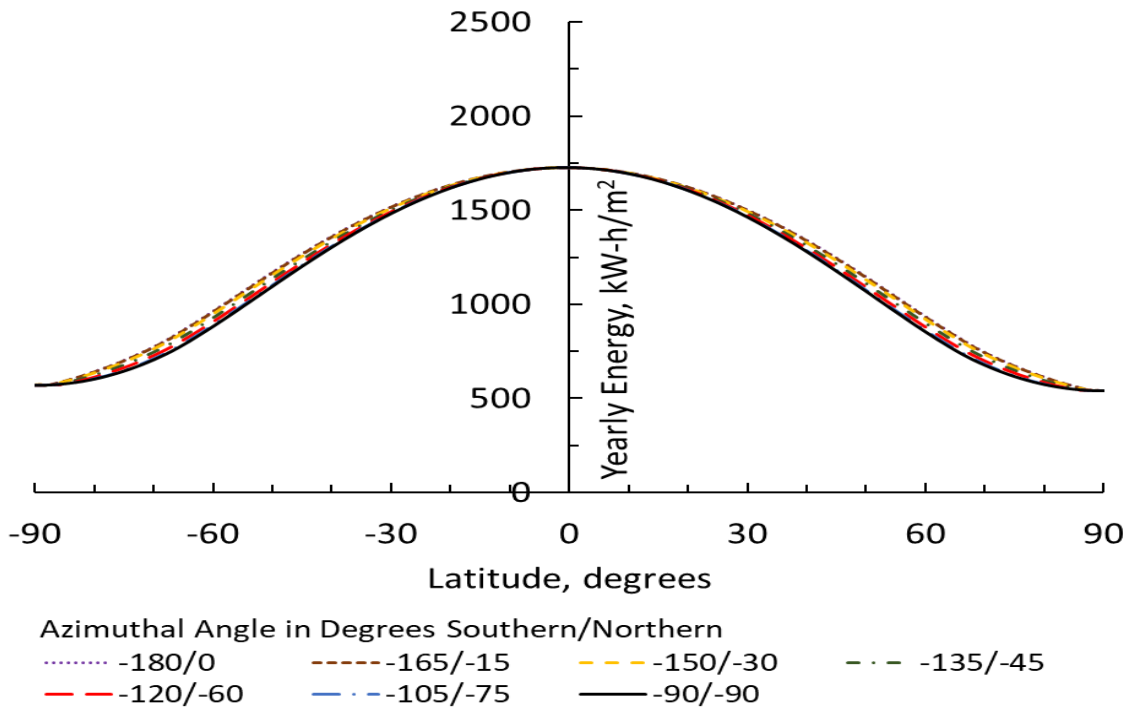


Figure 5.8: Yearly maximum intercepted energy for a uniform value of $N = 6$ throughout the year.

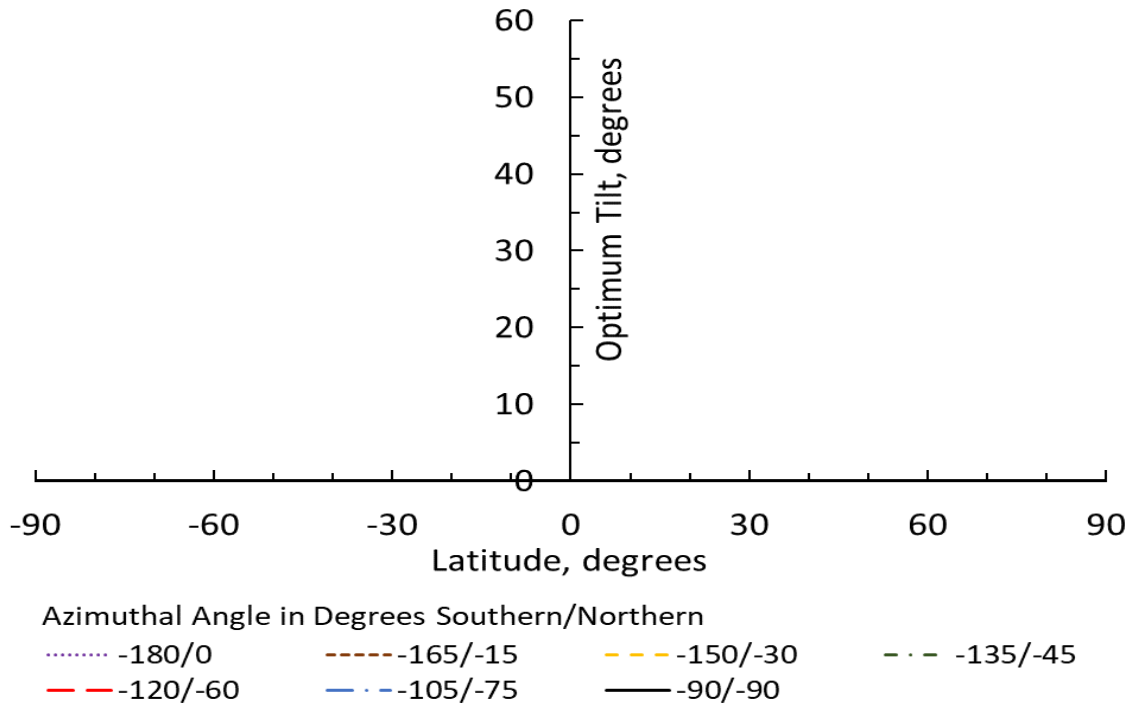


Figure 5.9: Yearly optimum tilt angles for a uniform value of $N = 8$ throughout the year.

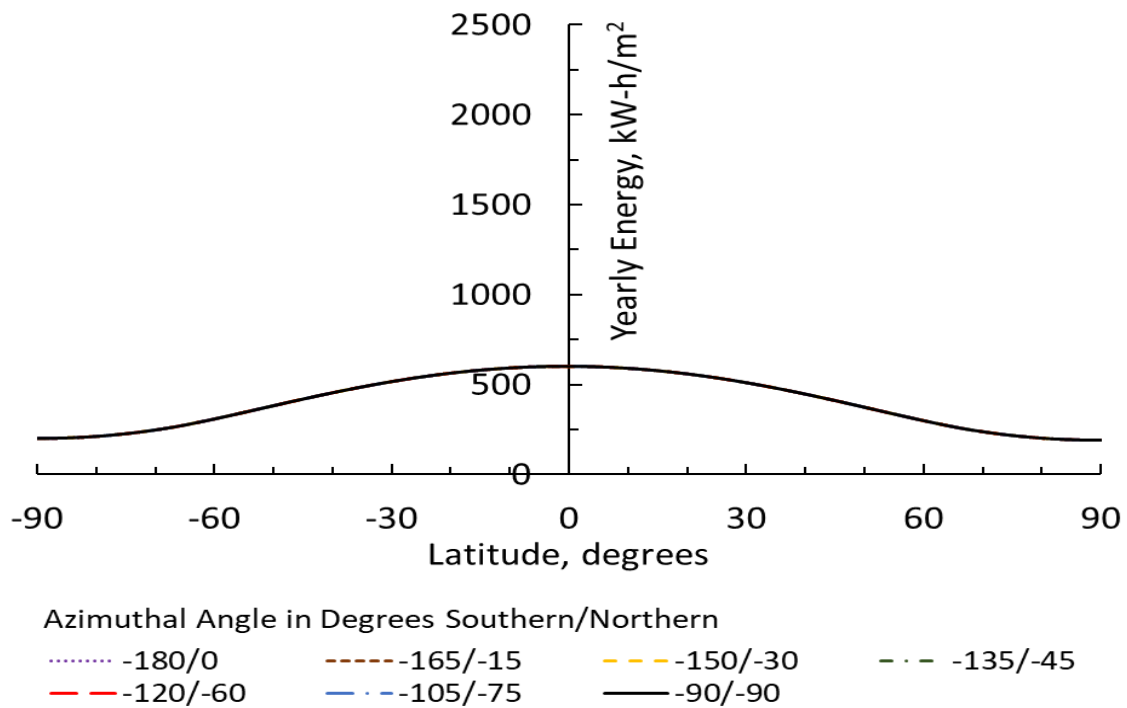


Figure 5.10: Yearly maximum intercepted energy for a uniform value of $N = 8$ throughout the year.

azimuthal angle. For each of the five Okta numbers presented, the optimum tilt angles are presented first, and the maximum incident energy is presented second. All optimum tilt angle graphs have the same range of values on both the vertical and horizontal axes. Likewise, all maximum incident energy graphs have the same range of values on the vertical and horizontal axes. This allows the reader to compare values between different graphs and determine the effects of cloud cover easier.

The five optimum tilt angle plots given for uniform yearly cloud conditions clearly show effects of increasing cloud cover. The optimum tilt plots show continual decreases in optimum tilt angle as cloud cover increases. The decreases are almost unnoticeable for Okta numbers from 0 to 2; but at an Okta number of 4 the decreases are more perceptible. For Okta numbers of 6 and 8 the differences are stark. At an Okta number of 6, the shapes of the curves change. For latitudes close to -90° and 90° the curves bend over and go to zero degrees at latitudes of -90° and 90° . The start of this bending behavior can be seen at an Okta number of 4. At an Okta number of 8, all optimum tilt angles are zero. This is true for all latitudes and all azimuthal orientations. It appears as if nothing is plotted in Figure 5.9, but as the legend shows, there are seven curves on this plot. They cannot be seen because they all lie right on the horizontal axis.

As expected, the maximum amounts of incident energy decrease as the cloud cover increases. For Okta numbers less than 2, these differences are almost unnoticeable, but become more noticeable and quicker as Okta numbers increase from 4. The incident energies at an Okta number of 8 are not zero, but are about 25% of those for clear skies. While the shape of the maximum energy curves does not change, the curves for different azimuthal orientations come closer together as the Okta number goes from 0 to 8. At 8 only one curve is seen, although all seven are plotted. For completely overcast skies, the azimuthal orientation has no effect on the results.

To get a better idea of the effects of cloud cover, Table 5.3 and Table 5.4 have been prepared. The quantities in these tables show the same trends as described above. From Table 5.3, it can be seen that the differences between the optimum tilt angles for $N = 0$ and $N = 2$ are fairly small with a slight increase with increase in latitude. The difference between the optimum tilt angles of $N = 2$ to $N = 4$ are larger, and this difference increases a significant amount with an increase in latitude. As more cloud cover is added, the differences between the optimum tilt angles increase. Ultimately the optimum tilt is 0° at all orientations when $N=8$. Table 5.4 represents the

maximum incident energy at different orientations, at different values of N. As more clouds are added the maximum energy values decrease. The highest values are seen at N=0 and the lowest at N=8, which is expected as the cloud cover reduces the solar radiation reaching the surface of the earth. It is to be noted that as more clouds are added to the atmosphere, there is a cumulative decrease in both the optimum tilt angle and the maximum incident energy.

The reason for the decreasing maximum incident energy values with increasing cloud cover is less solar energy makes it to the earth as the cloud cover increases. The reason the optimum tilt angle decreases is the solar energy mix between beam and diffuse is shifting towards more diffuse energy and less beam energy. This can be seen by studying Figure 4.4. For heavy cloud cover, the diffuse can dominate the beam energy. For an Okta number of 8 there is no beam solar energy reaching the surface of the earth; only diffuse solar energy is incident on the solar panel. This is why all optimum tilt angles at an Okta number of 8 are exactly zero degrees. In this case, the maximum energy is collected when the panel is horizontal and points directly towards the sky (see Figure 5.9). The maximum energy values shown in Figure 5.10 are the amount of diffuse energy for heavy cloud cover. It is this distribution between beam and diffuse energy that is the cause of the collapsing of the different azimuthal curves. Diffuse solar energy is the same in all directions, making the azimuthal orientation less important as the split between beam and diffuse energy shifts towards diffuse. Essentially the decreasing of the optimum tilt angles with increasing cloud cover is due to a shifting of the solar energy mix from beam to diffuse. The decrease in the maximum incident energy is due to a decrease in total energy reaching the surface of the earth.

Also evident in Figure 5.1 through Figure 5.10 is the effect of latitude on the optimum tilt angle and the maximum incident energy. Increasing the latitude location of the panels results in an increase in the optimum tilt angle. This trend is not seen for latitudes close to -90° or 90° for Okta numbers of 4 and 6 and is not seen at all for an Okta number of 8. Whenever the optimum tilt angle decreases with increasing latitude, this is due to the beam to diffuse energy ratio decreasing and is not an effect caused by latitude. The purest latitude effects can be seen in Figure 5.1 and Figure 5.2. In Figure 5.3 through Figure 5.10 some latitude effects are hidden by cloud effects. The beam to diffuse ratio is the largest in the clear sky results; and thus does not mask the effects of the latitude. The effect of latitude on maximum incident energy is obvious. Maximum incident energy is obtained slightly south of the equator, less than -1° , and less incident energy is obtained at latitudes that move outwards from the equator towards the poles.

Table 5.3: Effect of cloud cover on optimum tilt angles for different amounts of uniform cloud cover throughout the year.

Latitude, degrees	Azimuthal Angle, degrees	Optimum Tilt Angle for N = 0, degrees	Optimum Tilt Angle for N = 2, degrees	Optimum Tilt Angle for N = 4, degrees	Optimum Tilt Angle for N = 6, degrees	Optimum Tilt Angle for N = 8, degrees
0°	0°	0.54	0.52	0.46	0.33	0
-23°	0°	19.85	19.26	17.20	12.40	0
40°	-15°	33.99	33.09	29.86	21.97	0
-50°	-150°	38.45	37.41	33.69	24.57	0
60°	-45°	42.76	41.54	37.13	26.32	0
-67°	-120°	43.20	41.69	36.28	23.34	0
75°	-75°	47.07	45.18	38.16	10.63	0
-76°	-90°	45.11	0	0	0	0
77°	-90°	46.90	44.47	0	0	0
-84°	-90°	53.27	51.28	43.84	0	0

Table 5.4: Effect of cloud cover on maximum incident energy for different amounts of uniform cloud cover throughout the year.

Latitude, degrees	Azimuthal Angle, degrees	Optimum Energy for N = 0, kW-h/m ²	Optimum Energy for N = 2, kW-h/m ²	Optimum Energy for N = 4, kW-h/m ²	Optimum Energy for N = 6, kW-h/m ²	Optimum Energy for N = 8, kW-h/m ²
0°	0°	2407	2390	2236	1728	602
-23°	0°	2318	2292	2117	1606	552
40°	-15°	2065	2026	1828	1336	446
-50°	-150°	1825	1787	1600	1156	382
60°	-45°	1439	1407	1253	900	297
-67°	-120°	1208	1183	1063	777	262
75°	-75°	937	919	831	621	215
-76°	-90°	891	881	824	637	222
77°	-90°	843	830	774	590	208
-84°	-90°	849	833	754	583	203

The best understanding of the effect of azimuthal angle on optimum tilt angle and the maximum incident energy can be obtained from Figure 5.1 and Figure 5.2. Figure 5.1 shows a rather strong dependence of the optimum tilt angle on the azimuthal angle, especially for the larger azimuthal angles. As the azimuthal angles approach $-90^{\circ}/-90^{\circ}$ the panel is orientated due east. This means the panel is collecting energy well in the morning, but poorly in the afternoon. The best azimuthal angle of any fixed solar panel for maximum yearly energy interception is due south in the Northern Hemisphere and due north in the Southern Hemisphere. Rotating the panel to the east or the west will reduce the amount of energy intercepted. This reduction follows a cosine type dependence and therefore starts slow and increases faster as rotation to the east or west gets larger. It can also be noticed that all azimuthal angles produce the same optimum tilts at latitudes of -90° or 90° . This has to be the case because the only azimuthal orientation that can be obtained at the north pole is due south and that at the south pole is due north. The maximum intercepted energy graph in Figure 5.2 shows some dependence of the maximum energy on the azimuthal angle. The largest maximum energies are obtained at azimuthal angles of $-180^{\circ}/-0^{\circ}$ and the smallest are obtained at $-90^{\circ}/-90^{\circ}$. These differences are larger at the midlatitudes than towards the equator or towards the poles.

5.3. Semi-Annual Cloud Changes

This section deals with varying the Okta number from the summer to the winter. To make things simple only two seasons are used, and spring and fall are ignored. For the Northern Hemisphere, the Okta number is set equal to zero in the summer and to 6 in the winter. These mimic a number of locations around the world that tend to have cloudier conditions in the winter compared to the summer. For the Southern Hemisphere this is reversed, and the Okta number is set equal to 6 in the summer and to zero in the winter. Because the results in Figure 5.1 through Figure 5.10 indicate a high degree of symmetry between the Northern and Southern Hemispheres, there is no reason to present the same case for both hemispheres. For this reason, Figure 5.11 and Figure 5.12 have different cloud conditions for the two hemispheres.

It can be seen that the pattern followed by the optimum tilt angle values in the Northern Hemisphere shown in Figure 5.11 are very close to the patterns followed by optimum tilt angle values for yearly uniform cloud cover plots for $N = 0$ shown in Figure 5.1. Since $N = 0$ in the summer and $N = 6$ in the winter, there is no cloud cover in the summer and 75% cloud cover in

the winter. This indicates the summer energy collection is dominating these results. The winter has an effect because the semi-annual results are 5° to 10° less than those for the uniform cloud cover results. This is especially evident for latitudes less than or equal to 11° where the optimum tilt goes to zero. The maximum incident energy results for the semi-annual case shown in Figure 5.12 have a similar shape to the uniform cloud cover results shown in Figure 5.2. The higher Okta number in the winter has an effect making the semi-annual results around 300 kW-h/m^2 less than the uniform yearly results in Figure 5.2.

For the Southern Hemisphere the shape of the optimum tilt angle curves and the maximum intercepted energy curves shown in Figure 5.11 and Figure 5.12 respectively look like those of the $N = 6$ case of the uniform cloud cover results shown in Figure 5.7 and Figure 5.8 respectively. This time the optimum tilt angles are higher by 5° to 10° and the maximum intercepted energies are higher by about 300 kW-h/m^2 . The summer results with an Okta number of 6 are controlling the results with influence from the winter results with an Okta number of zero. For both the Southern and Northern Hemispheres, the summer conditions control the shape of the results because the days are longer in the summer.

5.4. Semi-Daily Cloud Changes

This section deals with varying values of N when two periods during the day are considered, namely morning and afternoon. $N=0$ in the mornings and $N=6$ in the afternoons in the Northern Hemisphere and vice-versa in the Southern Hemisphere. Because of symmetry, the transfer from morning to afternoon takes place at solar noon. Thus, morning runs from sunrise to solar noon and afternoon runs from solar noon to sunset.

Results for the optimum tilt angle for semi-daily changes in the Okta number are shown in Figure 5.13 and those for the maximum intercepted energy are shown in Figure 5.14. While it can be said that the Southern Hemisphere results take on shapes something like the uniform yearly values with a $N = 6$ value, there are more zero optimum tilts in the semi-daily results. The curves representing azimuthal angles of -90° , -105° , and -120° for the semi-daily results are composed of all zero values, as opposed to just the -90° results for the uniform yearly results. These zero valued curves are on Figure 5.13 but cannot be seen because they are underneath the horizontal axis. It is even harder to compare the Northern Hemisphere results to some case in the uniform yearly results.

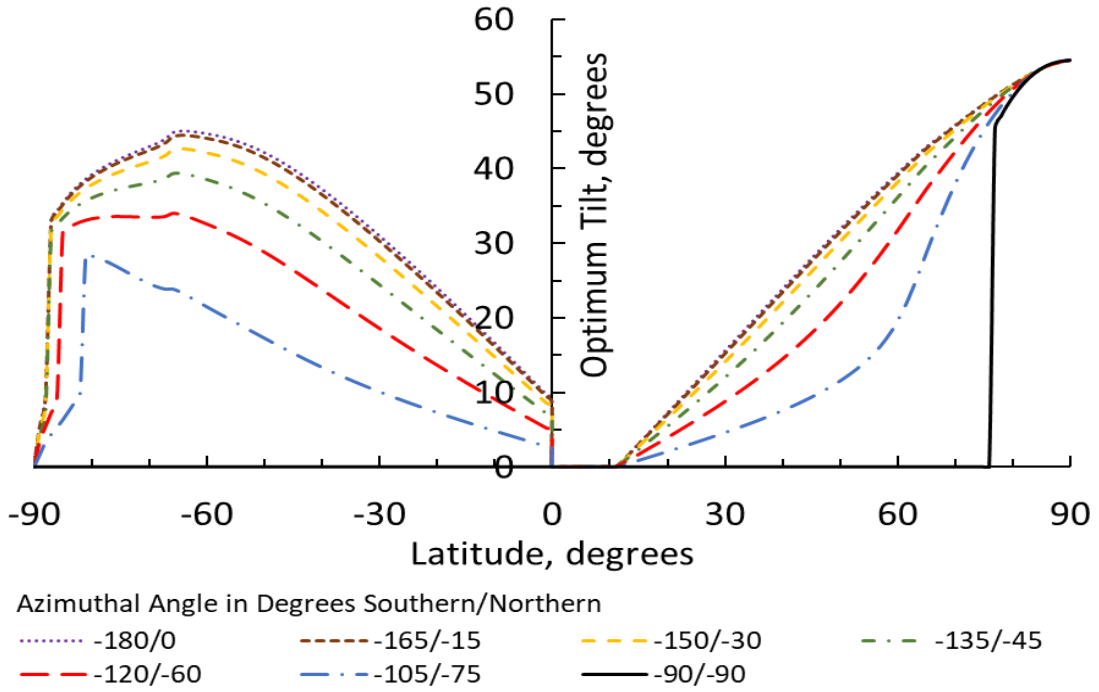


Figure 5.11: Optimum tilt angles for semi-annual varying values of N.

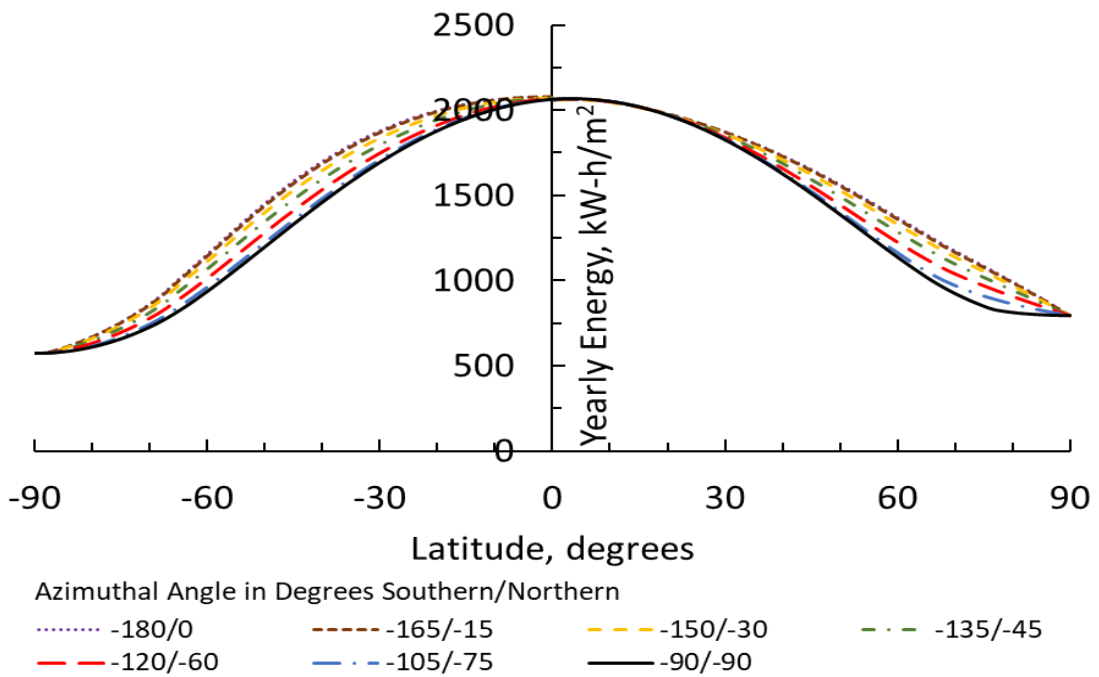


Figure 5.12: Yearly maximum intercepted energy for semi-annual varying values of N.

There are some unique features to the Northern Hemisphere semi daily results shown in Figure 5.14.

To understand the results in Figure 5.13 it is essential that one recognize that all azimuthal angles presented point the solar panel to the east. This means the Okta number used for morning cloud cover is more influential than the Okta number used for afternoon cloud cover. For the Southern Hemisphere the morning Okta number is 6, this is the reason that the results are tending to look like those in Figure 5.7 for optimum tilt angles and Figure 5.8 for the maximum intercepted energy. The Northern Hemisphere uses $N=0$ in the morning and thus does not have the drop to a 0° tilt at a latitude of 90° . The unique aspect of the Northern Hemisphere semi-daily results is curves for different azimuthal angles cross. This crossing behavior is also seen in the maximum intercepted energy values shown in Figure 5.14. Crossing behavior is interesting and has to have something to do with the large azimuthal angles picking up more energy from the morning sun at the low latitudes. The morning sun is predominately composed of beam radiation and the panel needs to point towards these beams of energy; while the afternoon is composed of more diffuse energy and the panel can be oriented over a range of tilts and still collect the bulk of the diffuse energy. It is the morning $N = 0$ value that is causing the low latitude, high azimuthal angled results to go to higher tilt angles than seen in Figure 5.1. It is interesting that the upward tilting of the 90° azimuthally orientated panel located on the equator makes it the top energy collector of all the panel azimuthal orientations at the equator. This was not seen in the uniform yearly results.

It also has to be noted that optimum tilt angles at the poles do not have the same optimum tilt angle. This is strange behavior because any azimuthal angle has the solar panel pointing due south at the north pole and due north at the south pole. These are the only directions that exist at the poles of the earth. The reason for these pole results is not one of orientation relative to due south or due north, but orientation relative to the time of the day. Because different cloud conditions are used in the morning and afternoon, the orientation of the panel at the poles affects whether the panel is seeing more or less morning sun; this is what causes the different results at the poles.

One more interesting observation of the Northern Hemisphere results is the opposite trends in going from one azimuthal orientation to another to those in the Southern Hemisphere and to those from the uniform yearly results. In general, the azimuthal results are the best for southward facing panels in the Northern Hemisphere and northward facing panels in the Southern

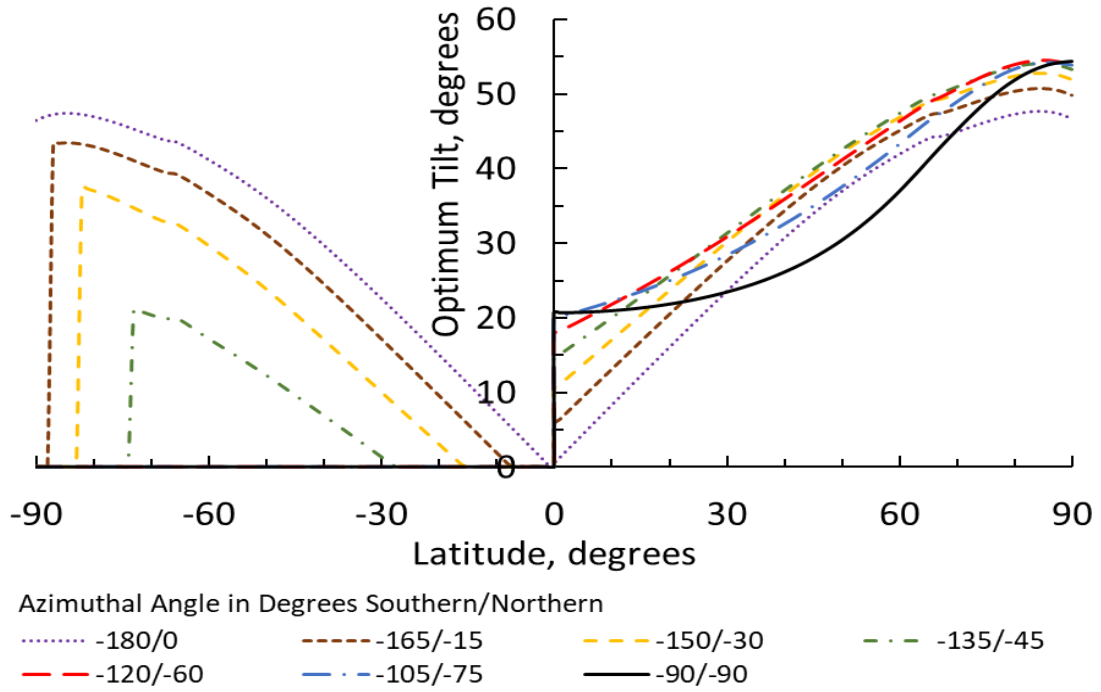


Figure 5.13: Optimum tilt angles for semi-daily varying values of N.

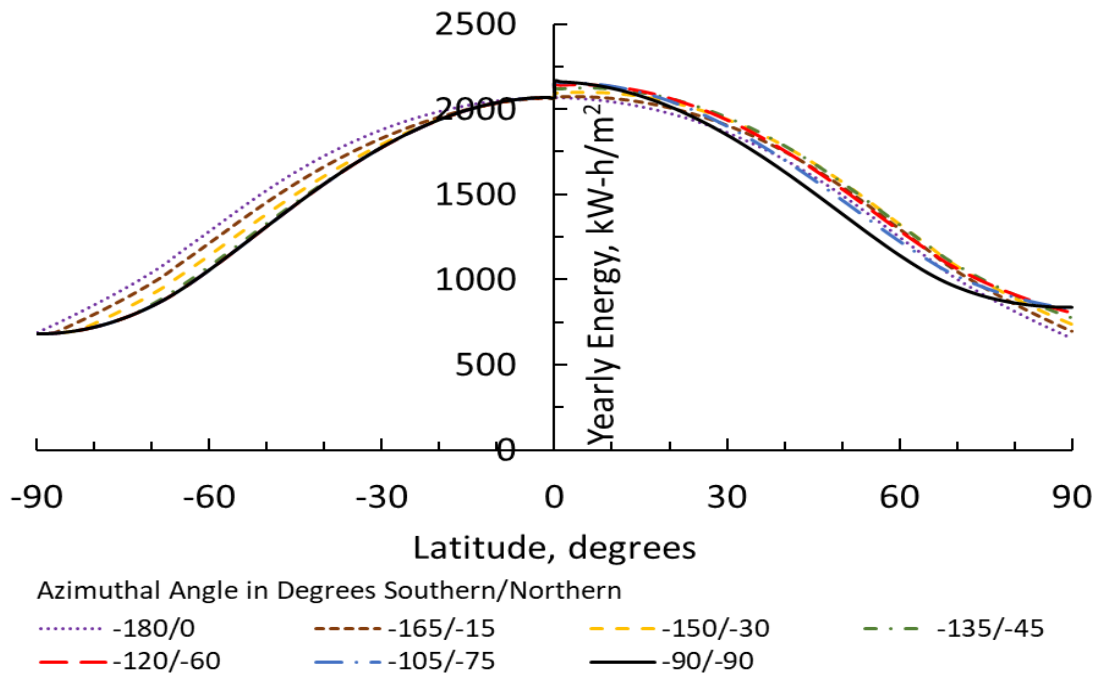


Figure 5.14: Maximum intercepted energy for semi-daily varying values of N.

Hemisphere. The Northern Hemisphere results in Figure 5.13 have mostly the opposite trend and those in Figure 5.14 have an up and down trend.

Chapter 6

Conclusions

The primary objective of this thesis work was to study the effect of cloud cover on the optimum tilt angle of a fixed solar panel for the purpose of achieving maximum incident energy on a yearly basis. As reported in Chapter 2, many studies have been done to determine optimum tilt angles at specific locations under typical meteorological conditions. This thesis deals with the effect of clouds producing results for every location on the surface of the Earth using latitude as a location variable. Longitude is not used as a location variable since the solar radiation received on a panel does not depend on longitude if whether effects are made uniform. For the results presented in this thesis, uniform whether conditions are assumed. A driving idea for this thesis work was to formulate a cloud cover model that can be used at any location in the world so that cloud cover can be controlled and studied. To the best of the author's knowledge, this thesis work is the first to accomplish this goal and present world-wide optimum tilt angles and maximum intercepted energy magnitudes. The analysis and results presented in this thesis shed light on the effect of cloud cover on optimum tilt angle at any latitude, for multiple azimuthal orientations.

6.1. Model Innovations

As part of this thesis work, a trigonometric, integral equation was derived to calculate the optimum tilt angle of a solar collector as a function of the latitude of panel location and azimuthal angle of the panel. Other parameters that are included in this mathematical model are the reflectivity of the ground, the beam transmissivity, and the diffuse transmissivity. By adjusting the

values of the transmissivities, the effect of cloud cover on the optimum tilt angle and the maximum incident solar energy can be studied. The optimum tilt angle equation used in this thesis follows the work done by Alhaidhari [12] for clear atmosphere conditions. The difference between the equation developed by Alhaidhari and that derived here is the inclusion of the change of panel sunrise and sunset with panel tilt angle. Alhaidhari excluded this effect on the optimum tilt angle. Including this effect in the optimum tilt angle model gives rise to a number of derivative of integral terms. For this reason, the difference between the optimum tilt angle equation developed as part of this work and the optimum tilt angle equation developed by Alhaidhari is referred to as the inclusion of the derivative of integral terms. Adding the derivative of integral terms to the optimum tilt angle equation greatly increases the complexity of the equations involved. The question this thesis has answered is whether the derivative of the integral terms affect the results to any important degree.

Because cloud effects enter the optimum tilt angle model through the beam and diffuse transmissivities, models for these transmissivities needed to be found. Alhaidhari [12] implemented sensible clear atmosphere transmissivity models developed by Hottel [24] and Liu and Jordan [18]. Neither of these models are capable of simulating cloud cover so an additional model had to be found. In this thesis, a cloud cover transmissivity model developed by Kasten and Czeplak [17] was used. Kasten and Czeplak developed equations for beam radiation and diffuse radiation in terms of the amount of cloud cover present in the sky. The amount of cloud cover is quantified by the Okta number, N , which varies from 0 to 8; 0 being a clear sky and 8 being a completely overcast sky. The Kasten and Czeplak cloud cover model is presented in terms of solar radiation values rather than transmissivities. Therefore, the first step was to convert these equations to beam and diffuse transmissivities. A second step was scrutinizing Kasten and Czeplak's clear sky model. The Kasten and Czeplak cloud cover model simply adjusts clear sky results to show the effects of clouds. Thus, Kasten and Czeplak model requires a clear sky model.

Kasten and Czeplak [17] utilized their own clear sky models. The problem with Kasten and Czeplak's models for clear sky beam and clear sky diffuse transmissivities was the values were unrealistic close to sunrise and sunset. Both the beam and diffuse transmissivity values near sunrise and sunset were negative. This is not physically possible. Also, some significant differences in magnitudes of the beam and diffuse transmissivities were seen between the Kasten and Czeplak models and those of Hottel [24] and Liu and Jordan [18]. According to Kasten and Czeplak, the

diffuse transmissivity follows the same trajectory as the beam transmissivity. According to Liu and Jordan, the diffuse transmissivity has a negative trend to the beam transmissivity. The Hottel equation for beam transmissivity and the Liu and Jordan equation for diffuse transmissivity are more realistic than the Kasten and Czeplak equations for clear sky conditions. Therefore, adjustments were made to the Kasten and Czeplak cloud cover model to use the Hottel and Liu and Jordan clear sky models, instead of the Kasten and Czeplak clear sky models. This was done by replacing the constants in the Kasten and Czeplak cloud model with quantities that satisfy the clear sky and overcast sky conditions at $N=0$ and $N=8$. The mathematical work for doing this is shown in detail in this thesis.

6.2. Optimum Tilt Angle and Incident Solar Energy Results

The first set of results presented were those comparing optimum tilt angles using the derivative of integral terms and those excluding the derivative of integral terms. This was done for the entire world. Results from the two models did not show any difference greater than 5×10^{-4} degrees, except in the case of the $-90^\circ/-90^\circ$ azimuthal angle orientations. For these azimuthal angles, the value of optimum tilt angle is 0° at the Equator and remains 0° until a particular latitude in both the Northern and Southern Hemispheres, at which time it quickly jumps to higher values. This abrupt change in optimum tilt occurred at a smaller latitude when the derivative of integral terms were included. While there were very significant differences in optimum tilt angles at these rapid change points, there was only small differences in maximum energy collected. Therefore, it is safe to conclude that the change of sunrise and sunset on the panel as a function of panel tilt angle can be excluded from the optimum tilt equation with essentially little difference in results. Doing this means a less complex equation can be utilized and the derivative of integral terms are no needed.

In this thesis, optimum tilt angle and maximum intercepted energy is calculated at various amounts of cloud cover from clear skies to completely overcast skies. The cloud cover conditions used were constant Okta numbers of $N = 0$, $N = 2$, $N = 4$, $N = 6$ and $N = 8$ for the entire year. Calculations were done from -90° latitude in the Southern Hemisphere to 90° latitude in the Northern Hemisphere in increments of 1° latitude for azimuthal orientations of $0^\circ/-180^\circ$, $-15^\circ/-165^\circ$, $-30^\circ/-150^\circ$, $-45^\circ/-135^\circ$, $-60^\circ/-120^\circ$, $-75^\circ/-105^\circ$, and $-90^\circ/-90^\circ$. The first number in each of these azimuthal orientations is for the Northern Hemisphere azimuthal orientations and the second

number is for the Southern Hemisphere azimuthal orientations. The azimuthal orientations of 0° - 180° are when the panel is pointed due south in the Northern Hemisphere and due north in the Southern Hemisphere. The other azimuthal orientations are when the panel is turned away from the 0° - 180° orientation in the eastward direction. No westward orientation results are shown in this thesis because they are almost identical to the corresponding eastward orientations.

As expected, the maximum optimum energy is found when $N = 0$ and the minimum optimum energy is found when $N = 8$. As cloud cover increases, the beam transmissivity decreases, but the diffuse transmissivity increases. Since more energy is received when $N = 0$, it can be said that beam transmissivity has the most impact on optimum energy. A very similar pattern is seen in the case of optimum tilt angles. When the amount of cloud cover increases, the optimum tilt angle decreases. This indicates that as the cloud cover increases, the diffuse transmissivity has more impact on the optimum tilt and the panel moves closer to a horizontal orientation to capture more diffuse radiation from the sky.

For all cases of Okta numbers except $N = 8$, the maximum intercepted energy was found at a -1° latitude and the largest optimum tilt angle was found at this location as well. The shapes of the plots are not perfectly symmetric around the Equator, but close. In the cases of $N = 0$, $N = 2$ and $N = 4$, the optimum tilt angle can be seen increasing with increasing latitude from the Equator, except for the -90° - 90° azimuthal angle where the optimum tilt remains 0° until a particular latitude, then jumps to a higher value, and keeps increasing with latitude from there. In the case of $N = 6$, the optimum tilt angle increases with latitude up to a particular value for each azimuthal angle and then decreases to 0° near the poles. In the case of -90° - 90° azimuthal angles, all the optimum tilt angles are equal to 0° . In the case of $N = 8$, the optimum tilt angle is equal to 0° at all latitudes, for all azimuthal orientations. This occurs because there is no beam radiation, and the panel collects the most diffuse radiation from the sky in the horizontal position.

The largest optimum tilt angle and optimum energy values are seen at the 0° - 180° azimuthal angle orientations. This is when the panel is facing due south in the Northern Hemisphere and due north in the Southern Hemisphere. When the panel is shifted away from these orientations, both the optimum tilt angle and the maximum intercepted energy values decrease. This is due to the fact that the 0° - 180° azimuthal orientations receive solar radiation in the morning and afternoon of the day equally. When the panel is shifted away from this orientation in an eastward direction, it is more difficult for the panel to receive beam radiation during the afternoon.

A similar reason is true for westward orientated panels. Due south and due north are the halfway points for the sun as it moves across the sky from morning to afternoon.

Along with cloud cover conditions that are uniform throughout the year, studies were done on semi-annual cloud changes and semi-daily cloud changes. These results used an Okta number of zero for one half and an Okta number of 6 for the other half. The semi-annual cloud cover results have different magnitudes than the uniform cloud cover results, but tend towards the shape of the uniform cloud cover results with an Okta number equal to that used during the summer half of the year. This is due to longer days in the summer half of the year compared to the winter half of the year. The semi-daily results show less resemblance to the uniform yearly cloud cover results than the semi-annual results.

References

- [1] K. Kirk, "Yale Climate Connections," 13 March 2020. [Online]. Available: <https://yaleclimateconnections.org/2020/03/burning-fossil-fuels-heats-the-climate-it-also-harms-public-health/>. [Accessed 05 April 2021].
- [2] "Lazard," 19 October 2020. [Online]. Available: <https://www.lazard.com/perspective/levelized-cost-of-energy-and-levelized-cost-of-storage-2020/>. [Accessed 05 April 2021].
- [3] W. F. Marion and A. P. Dobos, "Rotation angle for the optimum tracking of one-axis trackers," National Renewable Energy Laboratory, Golden, 2013.
- [4] "Solar Tracker," Wikipedia, [Online]. Available: https://en.wikipedia.org/wiki/Solar_tracker. [Accessed 05 April 2021].
- [5] H. Tan, "Go Green Solar," 24 July 2019. [Online]. Available: <https://blog.gogreensolar.com/2019/07/optimize-your-solar-production.html>. [Accessed 05 April 2021].
- [6] D. Mcgee, "Kiewit," [Online]. Available: <https://www.kiewit.com/plant-insider/current-issue/fixed-tilt-vs-axis-tracker-solar-panels/>. [Accessed 05 April 2021].
- [7] "Wikipedia," Price history of silicon PV cells since 1977, 2 November 2020. [Online]. Available: https://commons.wikimedia.org/wiki/File:Price_history_of_silicon_PV_cells_since_1977.svg. [Accessed 05 April 2021].
- [8] Y. S. Nakrani, "Optimum Angles for PV Panels for Different Conditions," Wright State University, Dayton, OH, 2015.
- [9] V. Medarapu, "Optimum Tilt Angle and Azimuthal Angle of a Solar PV Panel using One-Axis Tracking System at Different Conditions," Wright State University, Dayton, OH, 2016.
- [10] M. Gustafson, "A Computational Approach to Simulating the Performance of a 24-Hour," Dayton, OH, 2013.
- [11] G. S. Gugale, "Development of Analytical Equations for Optimum Tilt of Two-Axis and Single-Axis Rotating Solar Panels for Clear Atmosphere Conditions," Wright State University, Dayton, OH, 2016.
- [12] S. Alhaidari, "A Look at the Optimum Slope of a Fixed Solar Panel for Maximum Energy," Wright State University, Dayton, OH, 2017.

- [13] R. P. I. R. S. J. M. a. R. S. Perez, "Modeling Daylight Availability and Irradiance Components from Direct and Global Irradiance," *Solar Energy*, vol. 44, p. 271, 1990.
- [14] S. Wilcox and W. Marion, "Users Manual for TMY3 Data Sets," National Renewable Energy Laboratory, Golden, CO, 2008.
- [15] J. A. Duffie and W. A. Beckman, *Solar Engineering of Thermal Processes*, New York: Wiley, 1980, pp. 90-101.
- [16] M. Lave and J. Kleissl, "Optimum fixed orientations and benefits of tracking for capturing solar radiation in the continental United States," *Renewable Energy*, vol. 36, no. 3, pp. 1145-1152, 2011.
- [17] F. Kasten and G. Czeplak, "Solar and Terrestrial Radiation Dependent on the Amount and Type of Cloud," *Solar Energy*, vol. 24, pp. 177-189, 1979.
- [18] B. Y. Liu and R. C. Jordan, "The Interrelationship and Characteristic Distribution of Direct, Diffuse and Total Solar Radiation," *Solar Energy*, vol. 4, no. 3, pp. 1-19, 1960.
- [19] P. S. Koronakis, "On the choice of the angle of tilt for south facing solar collectors in the Athens basin area," *Solar Energy*, vol. 36, no. 3, pp. 217-225, 1986.
- [20] V. Badescu, "A new kind of cloudy sky model to compute instantaneous values of diffuse and global solar irradiance," *Theoretical and Applied Climatology*, vol. 72, pp. 127-136, 2002.
- [21] Y. Q. Tian, R. J. Davies-Colley, P. Gong and B. W. Thorrold, "Estimating solar radiation on slopes of arbitrary aspect," *Agricultural and Forest Meteorology*, vol. 109, no. 1, pp. 67-74, 2001.
- [22] K. P. Kathirvelu and B. Viswanathan, "Estimation of Optimum Tilt Angle of PV Panel for Maximum Energy Harvesting," *International Journal of Electrical and Computer Engineering*, vol. 6, no. 5, pp. 2016-2024, 2016.
- [23] D. T. Reindl, W. A. Beckman and J. A. J.A.Duffie, "Evaluation of hourly tilted surface radiation models," *Solar Energy*, vol. 45, no. 1, pp. 9-17, 1990.
- [24] H. C. Hottel, "A simple model for estimating the transmittance of direct solar radiation through clear atmospheres," *Solar Energy*, vol. 18, pp. 129-134, 1975.
- [25] N. Nijegorodov, "Improved ASHRAE model to predict hourly and daily solar radiation components in Botswana, Namibia, AND Zimbabwe," *Renewable Energy*, vol. 9, no. 1-4, pp. 1270-1273, 1996.
- [26] C. A. Gueymard, "Direct solar transmittance and irradiance predictions with broadband models. Part I: detailed theoretical performance assessment," *Solar Energy*, vol. 74, no. 5, pp. 355-379, 2003.
- [27] B. Haurwitz, "Insolation in relation to cloud type," *Journal of the Atmospheric Sciences*, vol. 3, no. 4, 1946.

- [28] S. Soulayman, "Economical and technical considerations for solar tracking: methodologies and opportunities for energy management," IGI Global, 2018, pp. 1-647.
- [29] L. T. Wong and W. K. Chow, "Solar radiation model," *Applied Energy, Elsevier*, vol. 69, no. 3, pp. 191-224, 201.
- [30] D. G. Erbs, S. A. Klein and J. A. Duffie, "Estimation of the Diffuse Radiation Fraction for Hourly, Daily, and Monthly-Average Global Radiation," *Solar Energy*, vol. 28, no. 4, pp. 293-302, 1982.
- [31] J. F. Orgill and K. G. T. Hollands, "Correlation equation for hourly diffuse radiation on a horizontal surface," *Solar Energy*, vol. 19, no. 4, pp. 357-359, 1977.
- [32] J. J. Carroll, "Global transmissivity and diffuse fraction of solar radiation for clear and cloudy skies as measured and as predicted by bulk transmissivity models," *Solar Energy*, vol. 35, no. 2, pp. 105-118, 1985.
- [33] R. E. Bird and C. Riordan, "Simple Solar Spectral Model for Direct and Diffuse Irradiance on Horizontal and Tilted Planes at the Earth's Surface for Cloudless Atmospheres," *Journal of Applied Meteorology and Climatology*, vol. 25, no. 1, pp. 87-97, 1986.
- [34] F. Y. Al-Aboosi, "Models and hierarchical methodologies for evaluating solar energy availability under different sky conditions toward enhancing concentrating solar collectors use: Texas as a case study," *International Journal of Energy and Environmental Engineering*, vol. 11, pp. 177-205, 2020.
- [35] E. R. Bird and L. R. Hulstrom, "Simplified Clear Sky Model for Direct and Diffuse Insolation on Horizontal Surfaces," Golden, CO, 1981.
- [36] N. Robinson, *Solar Radiation*, Elsevier, Amsterdam, 1966.
- [37] M. S. Ahamed, H. Guo and K. Tanino, "Evaluation of Cloud Cover Based Model for Simulation of Hourly Global Solar Radiation in Western Canada," *International Journal of Sustainable Energy*, vol. 38, no. 1, pp. 64-73, 2019.
- [38] R. Karkee, S. Khadka, G. Luitel, M. Devkota, B. Khadka, S. Sapkota and P. Bhetwal, "Comparing and Optimizing of Solar Insolation on Yearly, Monthly and Seasonally Basis for Solar Devices Performance in Nepal," *International Journal of New Technology and Research*, vol. 3, no. 1, pp. 26-33, 2017.
- [39] H. P. Garg, *Treatise on Solar Energy: Volume1: Fundamentals of Solar Energy*, Wiley, NY, 1982, pp. 375-381.
- [40] F. Jafarkazemi and S. A. Saadabadi, "Optimum tilt angle and orientation of solar surfaces in Abu Dhabi, UAE," *Renewable Energy*, vol. 56, pp. 44-49, 2013.

- [41] M. Kacira , M. Simsek , Y. Babur and S. Demirkol, "Determining optimum tilt angles and orientations of photovoltaic panels in Sanliurfa, Turkey," *Renewable Energy* , vol. 29, pp. 1265-1275, 2004.
- [42] M. J. Ahmad and G. N. Tiwari, "Optimization of Tilt Angle for Solar Collector to Receive Maximum Radiation," *The Open Renewable Energy Journal*, vol. 2, pp. 19-24, 2009.
- [43] E. Calabrò, "Determining optimum tilt angles of photovoltaic panels at typical north-tropical latitudes," *Journal of Renewable Sustainable Energy*, vol. 1, 2009.
- [44] B. Jamil , A. T. Siddiqui and N. Akhtar, "Estimation of solar radiation and optimum tilt angles for south-facing surfaces in Humid Subtropical Climatic Region of India," *Engineering Science and Technology, an International Journal*, vol. 19, pp. 1826-1835, 2016.
- [45] J. Kern and I. Harris, "On the Optimum Tilt of a Solar Collector," *Solar Energy*, vol. 17, pp. 97-102, 1975.
- [46] E. Asl-Soleimani , S. Farhangi and M. S. Zabihi, "The effect of tilt angle, air pollution on performance of photovoltaic systems in Tehran," *Renewable Energy*, vol. 24, pp. 459-468, 2001.
- [47] P. I. Raptis, S. Kazadzis , B. Psiloglou, N. Kouremeti , P. Kosmopoulos and A. Kazantzidis, "Measurements and model simulations of solar radiation at tilted planes, towards the maximization of energy capture," *Energy*, vol. 130, pp. 570-580, 2017.
- [48] "National Renewable Energy Laboratory," [Online]. Available: <https://www.nrel.gov/grid/solar-resource/renewable-resource-data.html>. [Accessed 05 April 2021].
- [49] B. Y. Liu and R. C. Jordan, "The Long-Term Average Performance of Flat-Plat Solar Energy Collectors," *Solar Energy*, vol. 7, p. 53, 1963.
- [50] "Leibnitz Integral Rule," Wikipedia, [Online]. Available: https://en.wikipedia.org/wiki/Leibniz_integral_rule. [Accessed 05 April 2021].
- [51] "Beer's Law," Britannica, [Online]. Available: <https://www.britannica.com/science/Beers-law>. [Accessed 05 April 2021].
- [52] T. Muneer, M. Gul and H. Kambezedis, "Evaluation of an all-sky meteorological radiation model against long-term measured hourly data," *Energy Conversion and Management*, vol. 39, no. 3-4, pp. 303-317, 1998.
- [53] J. K. Page, "Proposed quality control procedures for the Meteorological Office data tapes relating to global solar radiation, diffuse solar radiation, sunshine and cloud in the UK," Report FCIBSE, 1997.